EIT wave observations and modeling in the STEREO era

Andrei N. Zhukov [a,b,*]

[a] Solar–Terrestrial Center of Excellence – SIDC, Royal Observatory of Belgium, Avenue Circulaire 3, B-1180 Brussels, Belgium
[b] Skobeltsyn Institute of Nuclear Physics, Moscow State University, 119992 Moscow, Russia

ARTICLE INFO

ABSTRACT

"EIT waves" are large-scale bright fronts observed propagating in the solar corona in association with coronal mass ejections (CMEs). An overview of the observed properties of large-scale wave-like fronts in the solar atmosphere (Moreton waves, EIT waves and similar phenomena observed in other wavelengths) is presented. The models proposed to explain these phenomena are reviewed. A particular emphasis is put on the recent EIT wave observations made by the STEREO (Solar–TErrestrial RElations Observatory) mission launched in October 2006. New key observational results and their implications for EIT wave models are discussed. It is concluded that no single model can account for the large variety of observed EIT wave properties. Prospects for future investigations of this complex phenomenon are outlined.

© 2011 Elsevier Ltd. All rights reserved.

1. Historical introduction

Transient solar phenomena occur on a variety of spatial scales. It may be considered surprising that it was not the large-scale but the small-scale transient phenomena (sunspot and faculae evolution, granules, spicules, flares, etc.) that were discovered first. These phenomena are relatively easy to detect in observations of the photosphere and chromosphere. However, due to the high density of the photosphere and chromosphere, it is difficult to produce large-scale disturbances in these layers. As we now know, at large scales the corona is more variable than the lower layers of the solar atmosphere, but observations of the corona are difficult (e.g. Golub and Pasachoff, 2010). This is especially true for regular observations over long periods that are needed to catch relatively rare and transient eruptive solar phenomena.

Solar prominences were discovered a long time ago using solar eclipse observations. They were usually found to be limited in size. However, since the observations of giant prominence eruptions have been made (e.g. Pettit, 1919), it became clear that transient phenomena in the solar atmosphere can occur at a large scale (comparable to the solar radius). The discovery of type II bursts in dynamic radio spectra of the Sun (Wild and McCready, 1950) was another indication of large-scale disturbances in the solar corona (e.g. Nelson and Melrose, 1985), although the large-scale nature of type II radio bursts became clear only later, after interferometric observations (Weiss and Sheridan, 1962; Weiss, 1963) and radio imaging of their sources (Wild et al., 1968; Kai and McLean, 1968) were made. The first intrinsically large-scale transient phenomenon

discovered in the images of the solar atmosphere was Moreton wave (Moreton, 1960; Moreton and Ramsey, 1960). As it will be shown below, the link between EIT waves (that are the subject of the present review) and Moreton waves is still controversial. Nevertheless, very similar models are often applied to explain these two phenomena. It is thus instructive to start with a description of observations and modeling of Moreton waves.

Moreton waves are dark arc-shaped large-scale fronts propagating in the solar chromosphere as observed in the center and wings of the Hα line at 6563 Å (e.g. Moreton, 1960; Eto et al., 2002; Warmuth et al., 2004a). The speed of Moreton waves can reach 800-1000 km s^{-1} and even larger (Moreton and Ramsey, 1960; Athay and Moreton, 1961). Moreton waves are observed to propagate up to 5×10^5 km from the flare site in a limited angular sector (e.g. Moreton, 1964), although a global propagation in all directions can sometimes be observed as well (Pick et al., 2005; Muhr et al., 2010). Sometimes the propagation of Moreton waves can be inferred from a sudden oscillation of a distant filament (e.g. Moreton and Ramsey, 1960; Moreton, 1964; Dodson and Hedeman, 1964; Smith and Harvey, 1971; Eto et al., 2002; Gilbert et al., 2008). Another key property of Moreton wave fronts is their visibility in the Hα line wings. The front detected in the blue wing of the line propagates immediately behind the front detected in the red wing (Moreton, 1964; Dodson and Hedeman, 1964; Eto et al., 2002). This implies that the chromosphere locally moves downward and then upward (at a speed of around 10 km s^{-1}) as the wave front propagates through it.

It can be easily seen that such a fast disturbance can hardly be explained by the propagation of a wave in the chromosphere. Indeed, taking typical chromospheric parameters (temperature $T = 10^4$ K, electron number density $n_e = 5 \times 10^{10}$ cm^{-3}, magnetic field $B = 10$ G), the sound speed is then $c_s = \sqrt{\gamma k T / m_p} \sim 12$ km s^{-1} and the Alfvén speed $v_A = B/\sqrt{4\pi m_p n_e} \sim 100$ km s^{-1} (k is the

* Correspondence address: Solar–Terrestrial Center of Excellence – SIDC, Royal Observatory of Belgium, Avenue Circulaire 3, B–1180 Brussels, Belgium.
Tel.: +32 2 790 3924.
E-mail address: Andrei.Zhukov@sidc.be

Boltzmann constant, $\gamma = 5/3$ is the ratio of specific heats and m_p is the proton mass). These values are at least an order of magnitude lower than the observed speeds. The occurrence of a very fast shock (with the Alfvén-Mach number $M_A \sim 10$) seems unlikely as the observed large distances of the wave propagation contradict the expected quick dissipation of such a shock (Uchida, 1968). This led to Meyer (1968) and Uchida (1968) conjecturing that the wave actually propagates in the corona, but produces the observed Moreton wave signatures as it encounters the chromosphere. Indeed, taking typical values for the coronal density (around $n = 10^8$ cm^{-3}) and temperature (around $T = 10^6$ K), and assuming a coronal magnetic field of around $B = 5$ G, the sound and Alfvén speeds are then $c_s \sim 120$ and $v_A \sim 1000$ km s^{-1}, respectively. Unlike the propagation of the Alfvén and slow magnetosonic waves, which strongly depends on the direction of the ambient magnetic field, fast magnetosonic (or fast-mode) waves propagate in all directions with respect to the magnetic field at a speed given by the following equation:

$$v_f^2 = \frac{1}{2}\left(v_A^2 + c_s^2 + \sqrt{(v_A^2 + c_s^2)^2 - 4v_A^2 c_s^2 \cos^2\theta} \right), \tag{1}$$

where θ is the angle between the direction of the wave propagation and the ambient magnetic field. A coronal medium with a low plasma beta is usually assumed ($\beta = 8\pi p/B^2 \sim c_s^2/v_A^2 \ll 1$, where p is the plasma pressure). It can be seen that in such a low-beta plasma the fast magnetosonic speed is of the order of the Alfvén speed.

Uchida (1968) solved linearized magnetohydrodynamic (MHD) equations and presented a detailed model of a fast magnetosonic wave propagating in the spherically symmetric corona with the radial magnetic field. Uchida's model adopted the short-wavelength, or WKB (Wentzel–Kramers–Brillouin) approximation assuming that coronal parameters do not change at the scale comparable to the wavelength. This approximation allowed Uchida (1968) to consider the problem in a similar way to that of geometrical acoustics (see e.g. Blokhintsev, 1981), so this approach can be called "geometrical magnetoacoustics". The wave propagates in the medium with inhomogeneous distribution of the characteristic speed (in this case, the fast magnetosonic speed), so its raypaths are curved as the wave is refracted away from high-Alfvén speed regions. In the configuration described by Uchida (1968), the wave packets are refracted downward and eventually reach the surface, producing the down-up swing of the chromosphere in agreement with observations (Fig. 1).

Later, the model by Uchida (1968) was extended to more realistic configurations of coronal plasma and magnetic field parameters (Uchida et al., 1973). The narrow angular span of the Moreton wave propagation was explained via the reflection of the wave packets from the regions of high Alfvén speed (Uchida, 1970). Finally, a fast magnetosonic wave may steepen to form a shock wave. This shock may—under certain conditions—produce a radio type II burst (see e.g. Nelson and Melrose, 1985). Early imaging observations of type II source positions roughly agreed with locations where the fast magnetosonic wave was expected to be shocked due to local minima of the coronal Alfvén speed (Uchida, 1974). Observational data confirm a high association between type II bursts and Moreton waves (e.g. Smith and Harvey, 1971; Harvey et al., 1974; Thompson et al., 2000b; Warmuth et al., 2004b; Warmuth, 2010).

The works by Uchida (1968, 1970) represent a prediction of the existence of large-scale coronal fast magnetosonic waves. Imaging observations of type II burst sources allowed us to make early tests of this prediction, with some success. Another test of this prediction was made when routine high-cadence observations of the solar corona became available in the 1990s with the advent of the Yohkoh and SOHO missions.
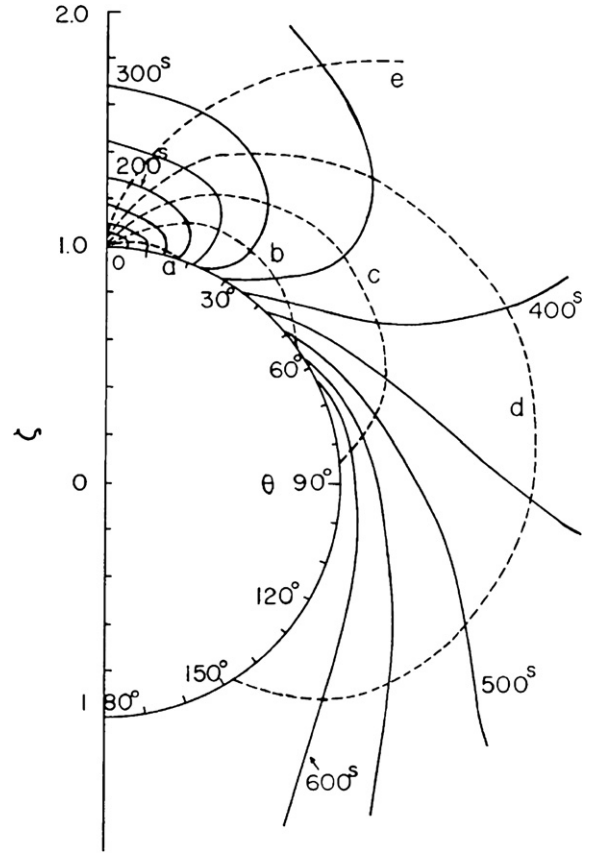
Fig. 1. Several representative paths of fast magnetosonic wave packets (dashed lines) propagating in the solar corona as calculated by Uchida (1968). The circle of a radius $\zeta = 1.0$ centered at $\zeta = 0$ is the solar surface. Solid lines represent corresponding wave fronts. The source of the wave is located at $\zeta = 1.0$, $\theta = 0°$. Note that the wave packets are deflected downward (towards the solar surface). From Uchida (1968).

2. Pre-STEREO observations of EIT waves

The first years of coronal observations made by the Yohkoh Soft X-ray Telescope (SXT, see Tsuneta et al., 1991) did not result in detection of large-scale coronal waves. However, the observations made by the Extreme-ultraviolet Imaging Telescope (EIT, see Delaboudinière et al., 1995) onboard the Solar and Heliospheric Observatory (SOHO) produced a drastically different result. Coronal images taken in the 195 Å extreme-ultraviolet (EUV) bandpass dominated by the Fe XII emission line (peak formation temperature around 1.5 MK) showed the occurrence of large-scale wave-like events (Thompson et al., 1998, 1999), see Fig. 2. As the waves were discovered in the EIT data, they were named "EIT waves".[1] For earlier reviews of EIT waves, see e.g. Zhukov (2004), Warmuth (2007), Wills-Davey and Attrill (2009) and Gallagher and Long (2010).

2.1. Interpreting EIT images

The interpretation of data taken by an EUV imager like SOHO/EIT will be briefly described in this section. The intensity of a coronal collisionally excited optically thin spectral line can be written as follows (e.g. Phillips et al., 2008):

$$I_\lambda = \int_h G(T, n_e) n_e^2 \, dh, \tag{2}$$

---

[1] EIT waves were briefly mentioned in earlier works by Moses et al. (1997) and Dere et al. (1997a), but the work by Thompson et al. (1998) was the first to present a detailed analysis of the EIT wave phenomenon.
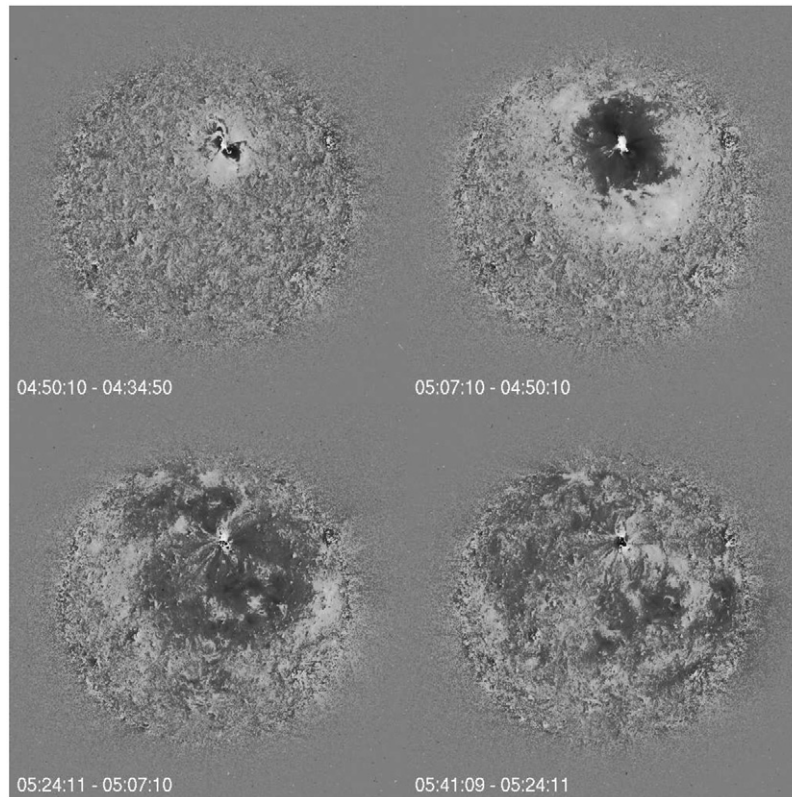
Fig. 2. Typical EIT wave event observed by SOHO/EIT on May 12, 1997 in the Fe XII (195 Å) bandpass. Running difference images (the previous image is subtracted from the current image) are shown to increase the visibility of the weak wave front. All times are UT.

where I_λ is the line intensity, $G(T, n_e)$ is the contribution function (that depends on the atomic parameters and elemental abundances), and the integration is made along the line of sight coordinate h. A useful quantity $\psi = \int_h n_e^2 dh$ is called the emission measure. The intensity measured by a wide bandpass EUV imager like SOHO/EIT can then be obtained as an integral of the spectrum (containing many spectral lines) with the weighting factor corresponding to the spectral bandpass response (with a typical width of the order of 10 Å). The interpretation of the EUV imager data is thus complicated as the detected intensity depends on a combination of temperature and density of the coronal plasma. As a zero-order approximation, one can assume that the radiation is integrated only along the hydrostatic pressure scale height H (e.g. Wills-Davey, 2006) and, with an average constant density n_e, the intensity becomes

$$I \sim G(T, n_e) n_e^2 H \qquad (3)$$

and the emission measure becomes $\psi = n_e^2 H$. For simplicity, one can also assume that in the quiet Sun the 195 Å bandpass of EIT is dominated by its strongest line (Fe XII at 195.12 Å), see Del Zanna et al. (2003). This line is formed in a relatively narrow temperature interval (between 1.2 and 1.8 MK, peaking around 1.4 MK, see e.g. Feldman et al., 1999 and Fig. 3). The contribution function of this line only weakly depends on density (Fig. 3), so $G(T, n_e) \approx G(T)$. As the hydrostatic pressure scale height H is proportional to the temperature T, then the relative intensity change can be written as

$$\frac{I_2}{I_1} \sim \frac{n_{e2}^2}{n_{e1}^2} \frac{G(T_2)}{G(T_1)} \frac{T_2}{T_1}, \qquad (4)$$

with subscripts 1 and 2 denoting parameters in the initial and final state, respectively. The peak of the coronal differential emission measure distribution (see e.g. Brosius et al., 1996) is situated close to the peak of the contribution function for the Fe XII line at

195.12 Å, and the contribution function $G(T)$ only weakly depends on temperature T near its peak (Fig. 3). Then a small temperature change (a few tens of percent) changes the contribution function only sightly and it can be assumed that $G(T_2) \approx G(T_1)$. The relative intensity change I_2/I_1 is then a linear function of the relative temperature change T_2/T_1 and a quadratic function of the relative density change n_{e2}/n_{e1}. The intensity is thus more sensitive to the density than to the temperature. Neglecting for simplicity the generally unknown temperature change (that is assumed to be small), one can interpret the relative intensity change in a bandpass I_2/I_1 over a pixel in terms of only a relative density change n_{e2}/n_{e1}:

$$\frac{n_{e2}}{n_{e1}} \approx \sqrt{\frac{I_2}{I_1}}. \qquad (5)$$

Another example is the adiabatic approximation with $T n_e^{1-\gamma} = const$. This means that a 30% increase in plasma density leads to around 20% increase in temperature. As one can see from the CHIANTI atomic database (Dere et al., 1997b, 2009) and Fig. 3, a 20% increase of temperature (in comparison with the peak formation temperature) leads to around 20% decrease of the contribution function of the Fe XII line at 195.12 Å. Therefore, in the case of weak adiabatic compression, the increase of temperature and the decrease of the contribution function can partially compensate each other in Eq. (4), and the approximate equation (5) can still be applied.

It needs to be stressed that Eqs. (3)–(5) have to be applied with caution. The assumptions that lead to them are not always fulfilled in realistic coronal conditions. Namely, the hydrostatic approximation sometimes cannot be used, for example to describe dynamic coronal structures (e.g. Aschwanden et al., 2001). Furthermore, spectroscopic observations (e.g. Del Zanna et al., 2003) demonstrate that EUV bandpasses may have a rather wide temperature response for structures containing multi-temperature
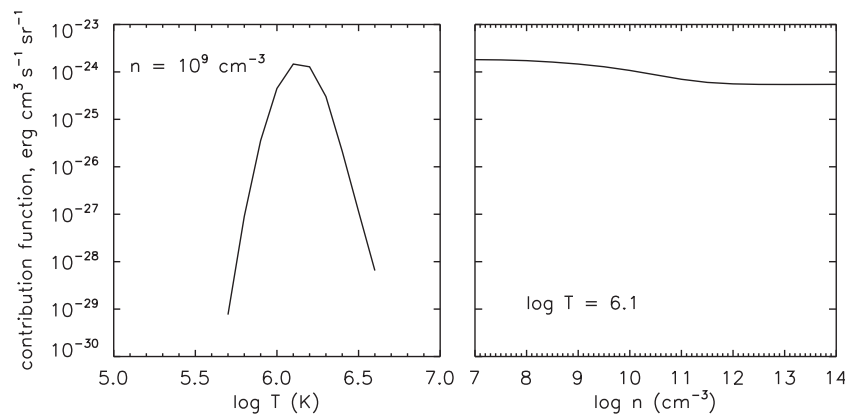
Fig. 3. Contribution function for the Fe XII line at 195.12 Å shown as a function of temperature at a constant electron density $n_e = 10^9$ cm^{-3} (left panel) and as a function of density at a constant temperature log$T = 6.1$ (right panel). The calculation was made using CHIANTI atomic database (Dere et al., 1997b, 2009) assuming ionization equilibrium values of Arnaud and Raymond (1992) and coronal abundances.

plasma, e.g. in coronal holes and polar plumes. In this case, the signal in the 195 Å EIT bandpass cannot be considered as formed mainly by a single Fe XII line. Finally, one cannot assume that the contribution function remains constant during processes leading to a strong heating or cooling. Temperature and density are coupled in the EUV observations of the corona and need to be disentangled using spectroscopic data. Therefore, Eq. (5) can only be used to obtain rough order of magnitude estimates.

2.2. Observed properties of EIT waves

EIT waves propagate across large areas of the quiet Sun, sometimes covering the whole visible solar disk. EIT waves do not propagate in coronal holes and active regions. They often have a quasi-circular shape (Fig. 2), although more complicated and rather irregular morphologies can also be observed, see e.g. Wills-Davey and Thompson (1999) and Fig. 4. In these cases, EIT waves often propagate along the large-scale magnetic field lines, i.e. in a rather narrow angular sector towards another active region (Delannée and Aulanier, 1999; Delannée, 2000). The EIT wave cross-section profile usually has the shape of a single pulse (Wills-Davey, 2003, 2006). Sometimes it can be modulated with a quasi-periodic function (Wills-Davey, 2003; Ballai et al., 2005; Wills-Davey, 2006). Quantitative measurements of the EIT wave profile evolution (Thompson et al., 1999; Wills-Davey, 2003, 2006; Warmuth, 2010) showed that the intensity contrast in EIT wave fronts may reach 60% (this corresponds to the density contrast of around 30%). The wave amplitude often decreases and the wave front width increases as the wave propagates (see e.g. Wills-Davey, 2003; Warmuth, 2010). This can be due to the wave expansion as it propagates in the spherical geometry (see e.g. Landau and Lifshitz, 1987). However, EIT wave propagation with a nearly constant wave profile was reported as well (Wills-Davey, 2006).

The EIT wave contrast is not homogeneous along its front (see Fig. 2). Moreover, it was shown that the contrast distribution along the front may vary with time, leading to an apparent "rotation" of the wave front (Podladchikova and Berghmans, 2005; Attrill et al., 2007). There is an indication that the sense of "rotation" is different for source active regions situated in different solar hemispheres: counterclockwise in the northern hemisphere and clockwise in the southern hemisphere (although the wave front "rotation" pattern was reported only in two events, see Attrill et al., 2007).

EIT waves are often associated with coronal dimmings, although one should not confuse these two phenomena. A dimming is a localized decrease of the coronal brightness that can be observed in soft X-rays (Rust and Hildner, 1976; Sterling and Hudson, 1997), in the EUV (Thompson et al., 1998, 2000a; Zhukov and Auchère, 2004) and probably in the white light (see a precursor work by Hansen et al., 1974). Dimmings are strongly associated with coronal mass ejections (CMEs), both spatially and temporally (Hudson and Webb, 1997; Dere et al., 1997a; Sterling and Hudson, 1997; Zarro et al., 1999; Thompson et al., 2000a; Hudson and Cliver, 2001). They represent the most frequent CME signature in the EUV corona (see Delannée et al., 2000). They are usually interpreted as regions of coronal mass evacuation during a CME eruption (e.g. Sterling and Hudson, 1997; Harrison and Lyons, 2000; Harrison et al., 2003; Zhukov and Auchère, 2004), and the angular extent of CMEs is observed to map well to the associated dimmings in the low corona (Thompson et al., 2000a). Dimmings are usually rather localized whereas EIT waves can exhibit a global propagation (see e.g. Thompson et al., 1998; Zhukov and Auchère, 2004 and Fig. 2). Global dimmings are sometimes observed (Zhukov and Veselovsky, 2007), but they are much more rare than global EIT waves. In some cases the dimming may initially immediately follow the EIT wave front (see Wills-Davey and Thompson, 1999 and Fig. 4).

EIT waves can be also observed in other EUV bandpasses, namely in the Fe IX/X 171 Å bandpass (Wills-Davey and Thompson, 1999) and in the Fe XV 284 Å bandpass (Zhukov and Auchère, 2004). During an EIT wave event observed nearly simultaneously in the 171 and 195 Å bandpasses of TRACE (transition region and coronal explorer, see Handy et al., 1999), the wave front contrast was significantly stronger in the 195 Å bandpass, see Wills-Davey and Thompson (1999) and Fig. 4. Coronal waves were also later observed in soft X-rays by SXT onboard Yohkoh (Khan and Aurass, 2002; Narukage et al., 2002) and by SXI (Soft X-ray Imager, see Hill et al., 2005) onboard GOES-12 (Warmuth et al., 2005). As it was shown by Hudson et al. (2003), detection of coronal waves in the Yohkoh/SXT data is hindered by the strong scattered light during flares.

Similar large-scale wave-like phenomenon was detected in the He I 10,830 Å line (Vršnak et al., 2002; Gilbert et al., 2004; Gilbert and Holzer, 2004). The physics of the line formation is complicated in the case of the He I line: it reflects the conditions in the chromosphere (collisional excitation) and corona (radiative excitation by the incident coronal radiation). The interpretation of these observations is thus controversial. Vršnak et al. (2002) conclude that the He I wave originates from the lower part of the true coronal wave front impacting the upper chromosphere and producing the observed wave signature via a collisional excitation mechanism. The formation of He I waves is then similar to that of Moreton waves. However, Gilbert et al. (2004) and Gilbert and Holzer (2004) interpret the He I wave as the "imprint" of the coronal compressive wave (EIT wave) generating the He I signal via the photoionization–recombination
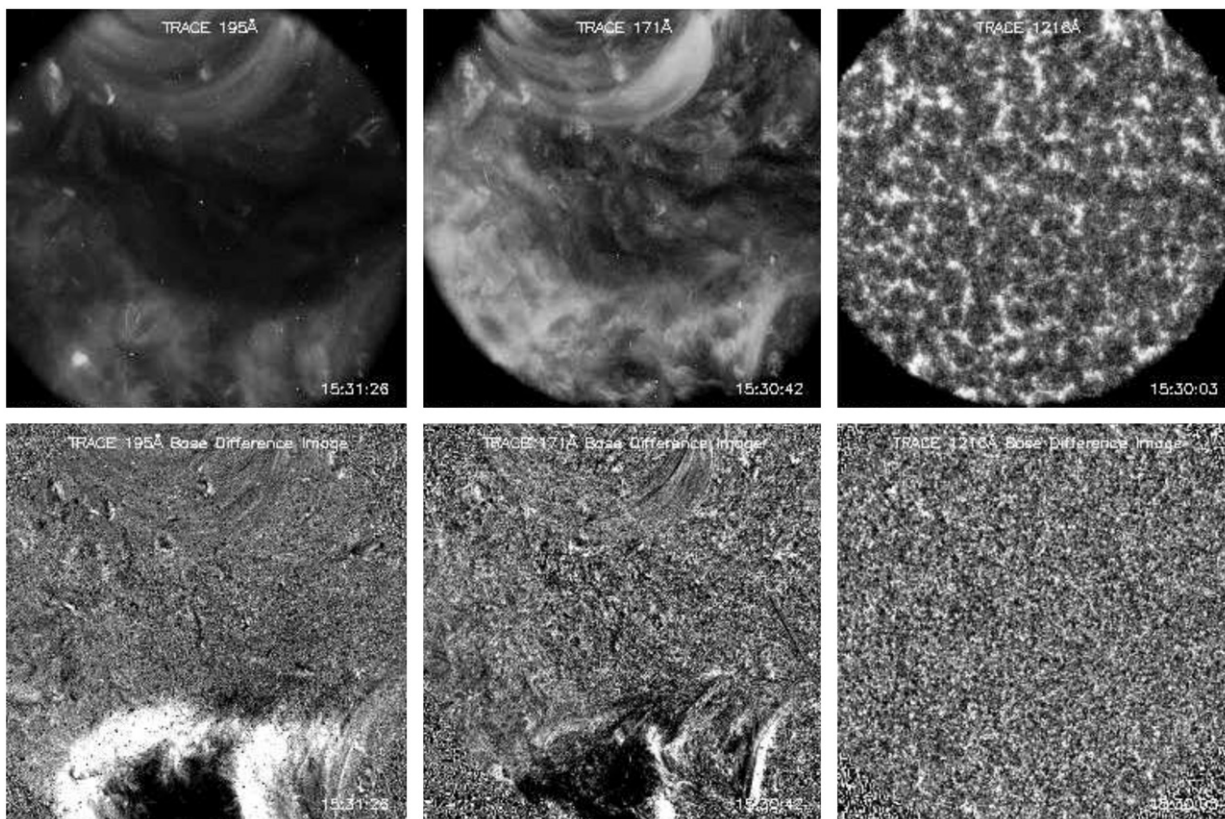
Fig. 4. A snapshot from the movie presented by Wills-Davey and Thompson (1999) showing the TRACE observations of the EIT wave event on June 13, 1998. Left, center and right columns are images taken in the 195, 171 and 1216 Å bandpasses, respectively. Top row contains normal (i.e. non-differenced) images and bottom row contains base difference images (i.e. the last pre-eruption image was subtracted from the original image). Note that the EIT wave front contrast is strongest in the 195 Å bandpass, and the absence of any wave signatures in the 1216 Å bandpass that contains chromospheric and lower transition region emission in the H I Lyα line.

mechanism. The coronal wave does not need to be refracted towards the chromosphere in this case.

EIT waves can also be detected by radio imaging at 17 and 34 GHz (Warmuth et al., 2004a; White and Thompson, 2005) and at metric wavelengths (Pohjolainen et al., 2001; Khan and Aurass, 2002; Vršnak et al., 2005). It is still unclear if all these diverse wave-like phenomena result from the same disturbance (fast magnetosonic wave, see Section 2.4).

Spectroscopic observations of EIT waves are very rare. This is mainly due to the difficulty of pointing a narrow spectrograph slit at the location (not known in advance) where the EIT wave will propagate. As reported by Harra and Sterling (2001, 2003), EIT waves could not be detected in two eruptive events observed by the Coronal Diagnostic Spectrometer (CDS, see Harrison et al., 1995). During a strong flare/CME event on December 13, 2006, the observations of the low corona dynamics made by the Extreme-ultraviolet Imaging Spectrometer (EIS, see Culhane et al., 2007) onboard Hinode showed a strongly blue-shifted feature that was interpreted as a possible signature of the fast-mode coronal shock wave (Asai et al., 2008). It was visible only in the hottest lines of the EIS data set (Fe XV and Ca XVII) and in soft X-rays, indicating that the temperature of the feature was greater than 2 MK. In this example, the front was traveling at a speed of around 650 km s^{-1} (as observed in soft X-rays), and it drifted through the EIS slit at a speed of around 460 km s^{-1}. The line-of-sight velocity in the front was rather high (around 100 km s^{-1}). As no detailed analysis of this feature was made by Asai et al. (2008), it is still unclear how this front relates to EIT waves (that are best observed in the Fe XII bandpass and are thus expected to be detected by EIS in the Fe XII line).

2.3. Stationary EIT wave fronts

Although the term "EIT wave" is usually applied to propagating bright fronts, stationary fronts that can also be observed in the EUV are sometimes called "EIT waves" as well (Delannée and Aulanier, 1999; Delannée, 2000). These stationary brightenings are seen after the main EIT wave passage. They can also be detected in the Hα data (Delannée et al., 2007). They are usually situated along the quasi-separatrix surfaces in the low corona (Delannée and Aulanier, 1999; Delannée et al., 2007) and may remain stable for several hours. These stationary bright fronts can be interpreted as signatures of plasma compression and heating at the quasi-separatrix surfaces due to the magnetic field line opening during the CME lift-off (Delannée and Aulanier, 1999; Delannée, 2000; Delannée et al., 2007).

Similar bright fronts moving at very low speeds (and eventually stopping) were observed by EIT as well (Thompson et al., 1998) in association with CME and EIT wave events. These fronts are interpreted as a signature of interchange reconnection between the CME large-scale field lines and oppositely directed magnetic field in a neighboring coronal hole (Crooker and Webb, 2006; Attrill et al., 2006). They stop after propagating along a very short distance that is much smaller than global EIT wave scales (Thompson et al., 1998; Crooker and Webb, 2006; Attrill et al., 2006). Stationary fronts will not be further considered in this review.

2.4. Relation between EIT and Moreton waves

After the EIT wave discovery, it was immediately suggested that the coronal fast magnetosonic wave predicted by Uchida (1968)

was finally observed (Moses et al., 1997; Thompson et al., 1999, 2000b). This interpretation was based on two main arguments. Firstly, EIT waves are compressive (see Section 2.2). Secondly, EIT waves can propagate in all directions from the eruption site. In the lower corona of the quiet Sun and away from large-scale magnetic neutral lines, the magnetic field is approximately radial. This is confirmed by EIT observations of ubiquitous nearly radial field-aligned structures above the limb. EIT waves can therefore propagate nearly perpendicular to the coronal magnetic field, similar to fast magnetosonic waves.

It, however, quickly became clear that the observed properties of EIT waves are very different from those of Moreton waves. The most drastic difference is that of the speed. EIT wave velocities are typically around $250\,km\,s^{-1}$, and they almost never exceed $450\,km\,s^{-1}$ in EIT data (Klassen et al., 2000; Wills-Davey et al., 2007; Thompson and Myers, 2009), whereas typical Moreton wave velocities are around $1000\,km\,s^{-1}$ (Moreton and Ramsey, 1960; Athay and Moreton, 1961). Another important difference is that EIT waves can have a quasi-circular shape (like that shown in Fig. 2), whereas Moreton waves propagate in a rather limited angular span (e.g. Moreton, 1964; Pohjolainen et al., 2001). In general, Moreton waves are observed significantly less often than EIT waves (Thompson and Myers, 2009; Warmuth, 2010).

Nevertheless, for every Moreton wave with simultaneous EIT data available, an associated EIT wave front can be detected (e.g. Thompson et al., 2000b; Warmuth et al., 2004a; Veronig et al., 2006; Vršnak et al., 2006; Warmuth, 2010; Muhr et al., 2010). The EIT wave front generally has a wider angular extent than that of the Moreton wave, but there is always a section where one can observe the propagation of both waves.

A way to resolve the speed discrepancy was proposed by Warmuth et al. (2001). They noted that Moreton and EIT wave fronts in the two events were lying on the same kinematic curves and suggested that they may represent the observational signatures of the same propagating disturbance (fast magnetosonic wave). The difference in the speed is then due to the wave deceleration. Indeed, Moreton waves are usually observed close to the erupting active region, whereas EIT waves are propagating further on. In addition, the low cadence of the EIT data (typically around 12 min) does not allow a detailed tracking of the propagation of fast transient phenomena: a typical EIT wave is observed only in three to four frames (Fig. 2).

Later, the tendency for the wave to decelerate was confirmed for more events and it was suggested that all the wave-like phenomena observed in the EUV, Hα, soft X-rays, He I and radio waves are signatures of a single propagating fast magnetosonic wave (Warmuth et al., 2004a, 2004b; Warmuth, 2007, 2010). The first high-cadence observations of an EIT wave by TRACE showed that the EIT wave speed can be as large as $800\,km\,s^{-1}$, a speed which approaches that of Moreton waves (Wills-Davey and Thompson, 1999). However, Eto et al. (2002) reported an event when the Moreton wave position (inferred from oscillations of a distant filament) was ahead of the EIT wave position. This is the only event for which such a discrepancy has been reported. Nevertheless, the result obtained by Eto et al. (2002) demonstrates that measurements of the Moreton and EIT wave propagation are subject to a significant uncertainty. The same trajectory can be approximated either with a parabolic fit for a single decelerating fast magnetosonic wave (Warmuth et al., 2004a) or with two linear fits describing EIT and Moreton waves separately (Eto et al., 2002). White and Thompson (2005) described the propagation of an EIT wave cospatial with a similar wave detected in high-cadence radioheliograph data at 17 and 34 GHz. They demonstrated that the wave, moving at a speed of around $830\,km\,s^{-1}$, exhibited no signs of deceleration during 4 min of radio observations. As the only model of Moreton waves considers them as fast magnetosonic

waves (Uchida, 1968), the physical nature of EIT waves may have to be identified additionally (see Section 3).

Another way to explain the speed discrepancy is to assume that EIT and Moreton waves (as well as different EIT waves) may be produced by different physical mechanisms (see Section 3). A particular attention was devoted to the so-called "S-waves", i.e. those EIT waves that exhibit sharp wave fronts in contrast to the generally diffuse EIT wave fronts (Biesecker et al., 2002; Thompson and Myers, 2009). Biesecker et al. (2002) suggested that only S-waves (that constitute around 7% of 173 EIT waves observed during March 1997–June 1998 period) are the coronal counterparts of Moreton waves. It should be noted, however, that a sharp S-wave is always observed as a diffuse wave further away from the source active region.

It was shown that the EIT wave interaction with active region loops, as described by Wills-Davey and Thompson (1999) and modeled by Ofman and Thompson (2002) and Ofman (2007), leads to loop oscillations that were clearly induced by the incident EIT wave (cf. the association of loop oscillations with type II radio bursts reported by Hudson and Warmuth, 2004). This is a strong argument in favor of the wave interpretation of the EIT wave phenomenon. On the other hand, small-scale low-lying structures did not oscillate during the EIT wave passage, so Wills-Davey and Thompson (1999) concluded that the wave propagated above the transition region (see also the EIT wave observations in the 284 Å bandpass reported by Zhukov and Auchère, 2004). This fact is difficult to reconcile with a single fast magnetosonic wave front extending from the corona to the chromosphere.

2.5. What produces EIT waves?

Ever since Moreton and EIT waves were first observed, there has been a question about their origins. Flares and CMEs were suggested to be the possible processes responsible for the wave generation (see e.g. a review by Vršnak and Cliver, 2008). If one assumes that EIT waves are true fast magnetosonic waves, then it is possible to use a well-developed hydrodynamic and MHD wave theory to investigate this issue.

A localized thermal pressure pulse (that may represent a flare) can produce a freely propagating sound wave (or a fast magnetosonic wave in the MHD case) that may steepen to form a shock (see e.g. Landau and Lifshitz, 1987). A very strong shock produced in such a way is called a blast wave (Sedov, 1959). Alternatively, a spherically expanding body (that may represent a CME) creates a wave in front of it, and this wave can steepen to form a piston-driven shock (Sedov, 1959; Landau and Lifshitz, 1987). In the realistic case of a three-dimensional (3D) spherical geometry, the steepening is slow in comparison with an analogous 1D case (Landau and Lifshitz, 1987). Plasma dissipative processes (viscosity and heat conduction) must then be weak enough, so that the wave is not absorbed before the shock is formed. Finally, if a body (e.g. a CME) moves at a speed faster than the characteristic speed in the medium (sound speed in the hydrodynamic case and fast magnetosonic speed in the MHD case), then a bow shock forms. It separates the unperturbed ambient medium upstream of the body from the shocked medium downstream (Landau and Lifshitz, 1987).

A combination of these three distinct mechanisms is also possible. For example, CMEs usually exhibit both expansion and large-scale bulk motion (e.g. Schwenn et al., 2005). In this case the shock can be formed through a combination of piston-driven and bow-shock mechanisms. A temporary piston may act similar to the pressure pulse in the blast wave mechanism. The wave created by a temporary piston is first driven, and then it may propagate freely in a way similar to a blast wave.

The discussion on the relation between CMEs and flares has been going on for many years. Different studies favor the primary role of flares (e.g. Steinolfson et al., 1978; Dryer, 1982) or CMEs (e.g. Kahler, 1992) in the eruptive solar activity. Recent works lead to the view that flares do not cause CMEs, and CMEs do not cause flares. These two observational phenomena represent two manifestations of the rapid evolution of the solar magnetic field (e.g. Gosling, 1993; Harrison, 1996). As the free energy stored in the non-potential coronal magnetic field is released, it is converted into the thermal energy of the coronal plasma that is partly radiated away (thermal emission of a flare), into the kinetic energy of mass motions (CMEs and small-scale ejecta) and into the kinetic energy of accelerated particles. Such a partitioning of the conversion of the free magnetic energy is still not entirely clear quantitatively and may vary from one event to the other (see e.g. Emslie et al., 2004, 2005). The observational basis for this interpretation includes, for example, a closely related timing of a CME and a corresponding flare (Harrison, 1995), a close synchronization of the CME acceleration and flare impulsive phase (Zhang et al., 2001; Zhang and Dere, 2006), location of the EUV flare site below the erupting prominence (Dere et al., 1997a), and the simultaneous development of the coronal dimmings and the associated flare (Hudson et al., 1996; Hudson and Webb, 1997; Sterling and Hudson, 1997; Zarro et al., 1999).

Due to this situation, it is difficult to distinguish between different physical processes that cause the coronal wave formation (for a detailed discussion see e.g. Vršnak and Cliver, 2008). In particular, it proved difficult to establish the origin of Moreton or EIT waves based only on their relative timing with respect to the associated flare and CME (Warmuth, 2010). However, even with the situation of a close relation between flare and CME, one can still ask if a flare (by means of a thermal pressure pulse, see e.g. Parker, 1961) or a CME (by means of a piston-driven or a bow-shock mechanism, see e.g. Sedov, 1959; Landau and Lifshitz, 1987) may produce a large-scale propagating wave.

From the physical point of view, it is still not clear if a flare may produce a propagating fast magnetosonic wave due to a thermal pressure pulse. The low plasma beta, β, in active regions (e.g. Gary, 2001) makes the ignition of thermal blast waves difficult, as can be demonstrated by simple calculations (Vršnak and Cliver, 2008). However, in the framework of the currently accepted paradigm, flares result from the coronal magnetic field reconnection (e.g. Priest and Forbes, 2002). The magnetic field in the reconnection region may be small, and the plasma beta may consequently be high. The guide magnetic field component should be significantly smaller than the reconnecting field component in this case. Additionally, it was demonstrated that Moreton waves usually originate in the periphery of erupting active regions, where the magnetic field is not as strong as in the active region core (Warmuth et al., 2004a). Nevertheless, it has to be pointed out that numerical simulations of CME-driven waves are abundant (see e.g. recent works by Chen et al., 2002; Pomoell et al., 2008), which is contrary to the situation with numerical simulations of propagating blast waves produced by magnetic reconnection. Finally, another possible way for a flare to produce coronal shocks is by generating small-scale eruptions (Klein et al., 1999), in contrast to the thermal blast wave mechanism.

Grechnev et al. (2008) found that the propagation of the Moreton/EIT wave event on July 13, 2004 is best described by a hydrodynamic blast wave solution (Sedov, 1959). However, statistical studies demonstrate that the association rate between EIT waves and CMEs is higher than that between EIT waves and flares (Biesecker et al., 2002). Gilbert and Holzer (2004) reported an occurrence of multiple (up to five) waves in the He I line observed during a single flare/CME event. They argue that two waves are produced by the CME and the other three result from the flare. It was pointed out that weak flares are often observed in association with EIT waves (Delannée, 2000),

implying that some condition other than the flare pressure pulse (namely, a CME) is necessary to generate an EIT wave (Cliver et al., 2005). Finally, Chen (2006) investigated 14 strong flares (up to X-ray class X1.2) that should presumably produce strong pressure pulses, but did not have an associated CME. In neither of these events was an EIT wave observed. This strongly implies that EIT waves are produced by CMEs (Chen, 2006).

2.6. Relation of EIT waves with coronal shocks

Strong association of Moreton waves with type II radio bursts (e.g. Smith and Harvey, 1971; Harvey et al., 1974; Thompson et al., 2000b; Warmuth, 2010) incited investigations of possible EIT wave association with coronal shock waves. If EIT waves are true fast magnetosonic waves, one can ask a question if they are shocked or not. An overview of theoretical mechanisms of shock wave formation is presented in Section 2.5, and observational arguments will be discussed in this section.

Klassen et al. (2000) investigated the relation between EIT waves and type II radio bursts. An EIT wave was observed associated with 90% of type II bursts. However, the type II burst speeds are on average around three times greater than EIT wave speeds. Another statistical study (Biesecker et al., 2002) reported that many EIT waves are not accompanied by type II bursts. As demonstrated by radioheliograph observations, type II burst sources can be detected at the front of Moreton or EIT waves (Pohjolainen et al., 2001; Khan and Aurass, 2002; Vršnak et al., 2005). However, the morphology of EIT and Moreton waves on the one hand, and the morphology of type II burst sources on the other hand, are generally not similar. This indicates that the type II radio emission and EUV emission may come from different parts of the fast magnetosonic wave front.

CME-driven shock waves can also be detected by coronagraphs (Sheeley et al., 2000; Vourlidas et al., 2003; Eselevich and Eselevich, 2008; Ontiveros and Vourlidas, 2009). Unfortunately, the fields of view of the LASCO (Large Angle Spectroscopic Coronagraph, see Brueckner et al., 1995) and EIT instruments onboard SOHO have not overlapped since the loss of the LASCO C1 coronagraph in 1998. Combining together data sets obtained by these two instruments is therefore difficult. In an attempt to link an EIT wave with the shock wave observed higher in the corona, Tripathi and Raouafi (2007) reported observations of a CME that was detected by the UVCS (UltraViolet Coronagraph Spectrometer, see Kohl et al., 1995) and LASCO instruments onboard SOHO, in association with an EIT wave. A coronal streamer was deflected during the CME propagation, presumably by the CME-driven shock wave (cf. Sheeley et al., 2000). The UVCS data showed significantly broadened and Doppler-shifted coronal spectral lines, again indicating the presence of a shock wave (see e.g. Ciaravella et al., 2005). As the EIT wave was propagating in the same direction as the shock inferred from LASCO and UVCS observations, Tripathi and Raouafi (2007) concluded that the EIT wave in this event is most probably a CME-driven shock. However, a very low EIT wave speed in this event (55 km s^{-1}, i.e. lower than the coronal sound speed of around 150 km s^{-1}) makes this interpretation doubtful.

In summary, the speed discrepancy and generally different locations of EIT waves and type II radio burst sources indicate that a shocked part of the large-scale fast magnetosonic wave may not coincide with the EIT wave. The shocked part of the wave may be located in a different part of the overall wave structure, perhaps high in the corona.

3. EIT wave modeling before the STEREO era

A number of physical mechanisms were suggested to explain EIT waves, but only five of them have been developed into

quantitative model. These are the geometrical magnetoacoustics model by Wang (2000), the forward MHD simulation of a fast-mode blast wave by Wu et al. (2001), slow-mode wave simulation by Wang et al. (2009), field line opening model by Chen et al. (2002), and the electric current shell model by Delannée et al. (2008). In this Section, these models are reviewed and compared with observations. Several other proposed mechanisms are described as well.

3.1. Fast magnetosonic wave model

Three-dimensional (3D) simulations by Wang (2000) and Wu et al. (2001) describe the EIT wave phenomenon as a fast magnetosonic wave.

The simulation by Wang (2000) is based on the geometrical magnetoacoustics model developed by Uchida (1968). The key difference between the two simulations is the adopted value of the coronal plasma beta: $\beta < 1$ in the simulation by Uchida (1968) and $\beta \sim 1$ in the simulation by Wang (2000).

Wang (2000) used a realistic coronal magnetic field configuration obtained using the potential field source surface (PFSS) model. This simulation successfully describes the EIT wave speed and its avoidance of active regions and coronal holes: fast magnetosonic wave packets are simply reflected from these areas of high Alfvén speed, or refracted in the direction of decreasing fast magnetosonic speed (Fig. 5). The wave is refracted upward, which is different from the downward refraction in the Moreton wave simulation of Uchida (1968). The simulation by Wang (2000) thus cannot explain Moreton waves. Another problem for this simulation is the absence of global propagation. The wave is refracted upward before it reaches positions far from its source, i.e. from the erupting active region. Refraction in the upward direction is still to be observed in the solar corona.

Wu et al. (2001) simulated the propagation of a fast magnetosonic wave using a non-linear forward modeling approach. In a realistic coronal magnetic field configuration provided by the PFSS
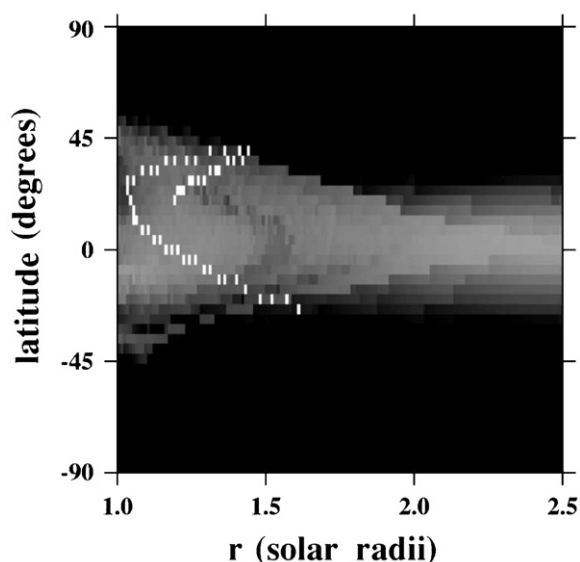
Fig. 5. Two representative paths of fast magnetosonic wave packets propagation (white pixels) in the solar corona as calculated by Wang (2000). The background image shows the distribution of coronal fast magnetosonic speed (black color denotes values higher than 500 km s^{-1}, light colors denote lower values) in the meridional plane (spherical coordinates r and θ). The source of wave packets is located at 22° north near the solar surface ($r = 1.0$). Note the upward wave packet refraction (away from the solar surface) and the wave reflection from a region of high fast-mode speed. From Wang (2000). Reproduced by permission of the American Astronomical Society (AAS).

model, they introduced a pressure pulse (simulating e.g. a flare). The pressure perturbation then propagates away as a fast magnetosonic wave. Again, in order to obtain the observed EIT wave speeds, Wu et al. (2001) adopted the quiet Sun coronal magnetic field values that produce high values of the plasma beta ($\beta > 1$). The global propagation of the fast-mode wave (dominated by the sonic component) well reproduces the observed EIT wave propagation (see Figure 4 in the paper by Wu et al., 2001).

Wu et al. (2005) developed a 3D non-linear MHD simulation of a large-scale wave propagation in a two-layer solar atmosphere (chromosphere and corona) with a simple dipolar magnetic field. A fast magnetosonic wave followed by a slow magnetosonic wave, both produced by a strong pressure pulse, were propagating in the corona. These two waves were followed by the second fast magnetosonic wave that was due to the switch-off of the pressure pulse. A rather low coronal plasma beta $\beta \sim 0.2$ was adopted by Wu et al. (2005), resulting in the Alfvén speed around 470 km s^{-1}. The waves did not refract back to the chromosphere, so the simulation by Wu et al. (2005) could not explain Moreton waves. Due to a simplified configuration of the solar atmosphere, no attempt was made to compare the simulation with an observed EIT wave event. However, multiple waves apparent in this simulation are potentially suited to explain multiple waves reported by Gilbert and Holzer (2004).

A crucial assumption for the fast-mode wave modeling is the value of the coronal plasma beta β in the quiet Sun areas. If low or high values of β are assumed, the resulting fast magnetosonic speed is close to the speed of Moreton or EIT waves, respectively. Direct observations of coronal magnetic field are difficult, so the value of β in the corona may be uncertain. It is often assumed that $\beta < 1$, but this statement usually applies to active regions (Gary, 2001). In the case of a force-free ($\beta \ll 1$) closed magnetic structure (an active region), the upward magnetic pressure is balanced by the downward magnetic tension force, and the upward plasma pressure is negligible. If $\beta \gtrsim 1$, then the plasma pressure cannot be neglected. The magnetic field then cannot constrain plasma, and the material would be free to escape to the interplanetary space in the form of solar wind, already from the low corona. This possibility does not agree with the current ideas about the acceleration of low-latitude slow solar wind (see e.g. Wang et al., 2000; Sakao et al., 2007).

The values of the coronal magnetic field in the quiet Sun are still uncertain, thus leading to a major uncertainty in the EIT wave modeling. Wu et al. (2001) note that the photospheric magnetograms used in their model have a low spatial resolution and thus cannot measure strong magnetic fields in sub-pixel magnetic field concentrations. The coronal magnetic field calculated via the PFSS model and the plasma beta may thus be underestimated and overestimated, respectively. This may be a problem for the EIT wave modeling in the fast magnetosonic wave framework.

In the models by Wang (2000) and Wu et al. (2001), the coronal fast magnetosonic speed smoothly varies from one location to the other. Murawski et al. (2001) considered the propagation of perpendicular fast magnetosonic waves in a structured corona. Only density inhomogeneities were taken into account. It was demonstrated that the fast magnetosonic wave speed in the inhomogeneous medium can be lower when compared with the homogeneous case. This may provide a solution to the problem of inconsistency between the low plasma beta and the low fast magnetosonic speed. No simulation in a realistic 2.5D or 3D geometry was made by Murawski et al. (2001), but the physical mechanism reported in this work appears promising for future investigations.

3.2. Field line opening model

As discussed in Section 3.1, high values of the coronal plasma beta, $\beta \sim 1$, in fast magnetosonic wave models may be considered

unrealistic. This led Chen et al. (2002) to develop another model in which EIT and Moreton waves represent different physical phenomena. Chen et al. (2002) performed a 2.5D numerical simulation of a sub-Alfvénic CME originating from a magnetic arcade in a low-beta ($\beta < 1$) corona. A cartoon illustrating this model is shown in Fig. 6. As the CME moves upward, it produces a fast magnetosonic wave in front of it. The wave may steepen to become a piston-driven shock if the local plasma conditions are favorable. The propagation speed of this piston-driven fast magnetosonic wave in the low corona is around 750 km s^{-1}, so it can describe the coronal counterpart of the Moreton wave (the interaction of this wave with the chromosphere was not modeled). Behind the fast magnetosonic wave, another density perturbation arises and propagates outward from the center of the arcade. It is produced due to the successive opening (from inside of the arcade to the outside) of magnetic field lines during the CME lift-off. As the central flux rope rises, it creates a deformation of large-scale field lines that propagates downward along the field lines at the Alfvén speed (Fig. 6). At the same time, the deformation is also transferred upward due to the continuous rise of the flux rope. It then propagates downward along the next field line. The disturbance resulting close to the solar surface is accompanied by plasma compression and thus may represent the "EIT wave". It is not a true magnetohydrodynamic wave. It propagates at a speed that is approximately three times smaller than the coronal fast magnetosonic speed. If the fast magnetosonic speed is around 750 km s^{-1}, then the EIT wave speed is around 250 km s^{-1}, which is in agreement with observations. As the EIT wave is produced by successive opening of field lines during the CME lift-off, at every moment it is cospatial with the legs of the CME frontal loop. A dimming corresponding to the plasma evacuation due to the CME is situated behind the EIT wave front (Chen et al., 2002).

The occurrence of this density perturbation that may be responsible for EIT waves was confirmed by Pomoell et al. (2008) in a numerical simulation very similar to that by Chen et al. (2002). Developing their model further, Chen et al. (2005a) used realistic values of coronal plasma and magnetic field parameters and for the first time created synthetic EIT and SXT images of a propagating EIT wave. It should be noted that both the fast-mode CME-driven wave and the slower EIT wave are visible in this simulation, contrary to the observations that show only one wave front in the corona (EIT wave).

The field line opening model of EIT waves developed by Chen et al. (2002) has several advantages over the fast-mode model. It adopts coronal plasma beta values that are probably more realistic ($\beta < 1$), see discussion in Section 3.1. It can also describe observed events in which EIT and Moreton waves probably represent different entities (e.g. Eto et al., 2002). The model by Chen et al. (2002) was also used to demonstrate that an EIT wave stops at coronal separatrix surfaces (Chen et al., 2005b), similar to what can sometimes be observed (Delannée and Aulanier, 1999; Delannée, 2000; Delannée et al., 2007). Finally, Chen (2009) reported an event observed by EIT and by the MK3 coronagraph and demonstrated that the EIT wave was cospatial with the legs of the CME frontal loop, in agreement with the prediction of the model by Chen et al. (2002).

An obvious drawback of the model by Chen et al. (2002) is its 2.5D configuration. It is not easy to imagine how such a mechanism would produce a nearly circular EIT wave front (see Fig. 2) in a realistic 3D magnetic field configuration. Another problem is the global propagation of EIT waves: to account for it, an initial arcade should have a very large dimension matching the region of the EIT wave propagation. Finally, EIT wave and coronal dimming are coupled in this model. The dimming is always located right behind the trailing boundary of the EIT wave front (Chen et al., 2002), whereas observations demonstrate that EIT waves can propagate to significantly larger distances than the extent of the coronal dimming (e.g. Thompson et al., 1998; Zhukov and Auchère, 2004). It should be also noted that in the synthetic EIT images calculated by Chen et al. (2005a) the EUV intensity perturbation generated via the field line opening mechanism propagates downward along the field lines. Such a downward motion is not observed.

Another problem may be linked to the quantitative description of the density perturbation in EIT waves. The simulated density increase in the EIT wave front is of the order of a few percent (see Figure 3 in the paper by Chen et al., 2002), which would produce up to 10% of the intensity increase (Eq. (5)). This is too small in comparison with observed values (several tens of percent). It is not clear what factors can influence the density change in an EIT wave front. It should be noted that this problem does not immediately arise in the model by Wu et al. (2001) as one can increase the amplitude of the initial pressure pulse to reach the desired density
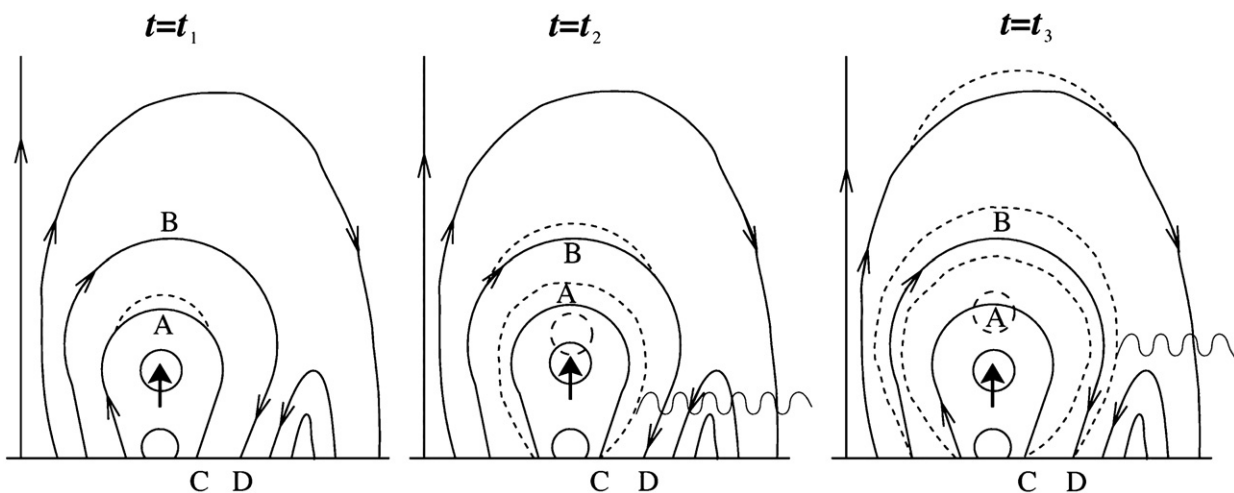
Fig. 6. A cartoon illustrating the numerical EIT wave model by Chen et al. (2002). Solid lines represent the initial configuration of the coronal magnetic field. Dashed lines show the progressive change of the coronal magnetic field during the CME lift-off. A central circle with a black arrow represents the rising motion of the CME flux rope (shown in cross-section). The field line deformation due to the CME lift-off propagates from the point A down to the solar surface (point C) at the Alfvén speed. It also propagates upward to create a deformation at point B. The deformation of a higher field line propagates from point B down to point D. Along the surface, we see the propagation of the EIT wave (field line deformation accompanied by plasma compression) from point C to point D. Wavy lines represent some of the fast magnetosonic waves produced at each moment by the coronal pressure perturbation. From Chen et al. (2002). Reproduced by permission of the AAS.

perturbation values, although the relation between the magnitude of the pressure pulse and the flare size is unclear.

Harra and Sterling (2003) reported an apparent confirmation of the model by Chen et al. (2002). An EIT wave event observed in the high-cadence TRACE data exhibited a possible signature of two structures: bright wave and weak wave. Harra and Sterling (2003) interpret the faster weak wave as a fast-mode wave, and the slower moving bright wave as an EIT wave produced via the field line opening mechanism developed by Chen et al. (2002). However, a careful inspection of the TRACE data shows that the bright wave appeared first, and the weak wave seemed to emanate from its front a bit later. This does not seem to be in agreement with the interpretation of the weak wave as a fast magnetosonic wave. The fast-mode MHD wave should have appeared right after the initial perturbation.

3.3. Slow magnetosonic wave model

As was mentioned in Section 2.4, EIT waves can propagate in all directions from the eruption site. EIT observations of nearly radial field-aligned structures in the lower corona of the quiet Sun above the limb demonstrate that the magnetic field away from large-scale magnetic neutral lines is approximately radial in the low corona. It is therefore assumed that EIT waves can propagate perpendicularly to the ambient magnetic field. This is one of the strong reasons to believe that they are fast magnetosonic waves. However, the speed of EIT waves can be close to the speed of the slow magnetosonic wave in the low-beta ($\beta < 1$) plasma, if the wave propagates obliquely with respect to the magnetic field (Wills-Davey et al., 2007; Krasnoselskikh and Podladchikova, 2007; Podladchikova et al., 2010). The speed of the slow magnetosonic wave can be written as

$$v_s^2 = \frac{1}{2}\left(v_A^2 + c_s^2 - \sqrt{(v_A^2 + c_s^2)^2 - 4v_A^2 c_s^2 \cos^2\theta}\right) \qquad (6)$$

Assuming $c_s \sim 120$ km s^{-1} and $v_A \sim 1000$ km s^{-1}, it can be found that $v_s \sim 100$ km s^{-1} for $\theta \sim 45°$. Such EIT wave speeds are sometimes observed (Thompson and Myers, 2009), but the existence of fields inclined to the radial direction at such an angle (and across surfaces comparable to the whole solar disc) is still to be demonstrated. In any case, slow magnetosonic speed cannot be higher than the coronal sound speed that is around 160 km s^{-1} at temperatures around 1.5 MK. Faster EIT waves can hardly be explained in the slow-mode wave framework.

Wang et al. (2009) used a numerical model setup similar to that by Chen et al. (2002) and investigated the wave-like phenomena behind the CME and the fast-mode CME-driven wave, with and without gravity. Due to limited computational resources, they adopted low values of the Alfvén speed (less than 50 km s^{-1}), thus resulting in $\beta > 1$. The fast magnetosonic CME-driven shock appears when the CME speed becomes higher than the fast magnetosonic speed. It is dominated by the sonic component (similar to the situation simulated by Wu et al., 2001). Its lower part sweeps the chromosphere and can produce the Moreton wave, as also shown in the simulation made by Chen et al. (2002). Behind the fast-mode shock, a slow-mode shock and velocity vortices appear at every side of the erupting flux rope. They propagate outwards at a speed that is around 40% that of the fast-mode wave. Wang et al. (2009) argued that the slow-mode shock and the velocity vortices represent the EIT wave.

The Moreton wave and EIT wave are two distinct physical entities in this model, and this explains their different speeds. However, it is not clear if the simulation results would be the same in the model atmosphere with the plasma beta $\beta < 1$ that would be more realistic according to Wang et al. (2009).

It is unclear if the mechanism proposed by Wang et al. (2009) would result in a nearly circular EIT wave front in a realistic 3D magnetic field configuration. The development of a 3D simulation is necessary. Again, similarly to the model by Chen et al. (2002), the CME-driven wave is well visible as a density perturbation, so it should be detected by EIT as well. The slow-mode shock and the velocity vortices are very weakly visible in density maps (see Figures 3 and 13 in the paper by Wang et al., 2009).

It should be noted that Rust and Svestka (1979) reported slowly propagating weak coronal X-ray disturbances and interpreted them as slow magnetosonic waves. These disturbances were observed in association with the filament disappearance or activation, sometimes without any flare. The disturbance propagation speed was decreasing from around 450 km s^{-1} down to around 15 km s^{-1} (Rust and Svestka, 1979). However, the time and place of the disturbance initiation was not observed in X-rays and was inferred by Rust and Svestka (1979) from other data (primarily chromospheric and radio). Therefore, the higher values of the speed are very uncertain. A simple calculation using their time-distance data shows that the speed of the front (moving from one observed position to the other) never exceeded 50 km s^{-1}. This phenomenon looks similar to EUV bright fronts produced by the interchange reconnection, see Section 2.3 and the works by Crooker and Webb (2006) and Attrill et al. (2006).

Slow magnetosonic waves were invoked by Gilbert and Holzer (2004) to explain large-scale waves detected in the He I line (see Section 2.2). They argued that the coronal fast magnetosonic wave propagating downward along quasi-radial magnetic field lines (e.g. Uchida, 1968) is essentially non-compressive in the linear regime. The chromospheric down-up motion detected in He I waves (as well as in Moreton waves) can be produced by slow magnetosonic waves that are generated by the pressure perturbation in the fast magnetosonic wave (Gilbert and Holzer, 2004). Note that a slow magnetosonic wave is always compressive.

3.4. Electric current shell model

Delannée et al. (2008) proposed an electric current shell model for EIT waves. A 3D flux rope is set to erupt producing a CME. Electric current sheets are formed at the interface between the flux rope and the ambient magnetic field. The resistive dissipation of the electric current leads to Joule heating of plasma that can be observed in the EUV as an increase of the emission measure in the 195 Å bandpass. In addition, a weak compression appears co-spatial with the current sheets. It is produced by the velocity field that, in turn, originates from the magnetic $\vec{j} \times \vec{B}$ force driving the flux rope eruption ($\vec{j}$ and $\vec{B}$ are the electric current and magnetic field vectors, respectively). A nearly circular shape was chosen for the initial flux rope configuration, in order to reproduce the quasi-symmetric shape of the observed EIT wave front. The current sheets expand together with the flux rope, and the current density may exhibit a time-dependent pattern due to the flux rope rotation. This may reproduce the time-dependent inhomogeneous structure of the EIT wave front (EIT wave "rotation") that is sometimes observed (see Section 2.2).

An advantage of this mechanism is the inclusion of both plasma heating and compression. Both of these factors are indeed at play, as it was shown using EIT wave observations in two bandpasses (Wills-Davey and Thompson, 1999). However, as is the case with other models, it is still not clear if heating and compression in the electric current shell mechanism are sufficient to produce the observed contrast of emission measure in the EIT wave fronts. It is also important to note that the erupting flux rope only expands together with its rising motion. Therefore, an important inference of the electric current shell model is that the EIT wave should be

observed at progressively larger heights. This is an important prediction that can be tested with STEREO (see Section 4.3).

3.5. Other interpretations of the EIT wave phenomenon

Several other EIT wave interpretations that are still not quantitative models will be briefly described here.

Wills-Davey et al. (2007) pointed out that several properties of observed EIT waves did not attract sufficient attention in models. Firstly, the large amplitude of many EIT waves (up to 30% density increase) makes the linear modeling (e.g. Uchida, 1968; Wang, 2000) questionable. Secondly, some EIT waves propagate with a constant wave profile (Wills-Davey, 2003). Wills-Davey et al. (2007) argued that a soliton description should be applied to the EIT wave phenomenon. In solitary waves (or solitons), a non-linear steepening of the wave front is balanced by the dispersion (that tends to widen the front), resulting in a constant wave profile. Taking into account the fact that speeds of many EIT waves are too low to be explained in the framework of the fast-mode wave mechanism, Wills-Davey et al. (2007) suggested that EIT waves can be explained as slow-mode solitons. The solitary wave framework is promising to explain some properties of EIT waves, although a quantitative model of the soliton propagation in the solar corona is still to be developed.

Attrill et al. (2007) suggested that the reconnection of the outer magnetic field of an expanding CME with favorably oriented small-scale quiet Sun loops may produce the observed signatures of the EIT wave propagation. However, the large-scale magnetic topology is not taken into account in this interpretation. Delannée (2009) demonstrated that, if a realistic large-scale magnetic field topology is taken into account, reconnection of the CME magnetic field with the small-scale quiet Sun field cannot occur. The large-scale field will simply not allow the CME field to encounter any small-scale field. The reconnection between the CME magnetic field and the ambient field can occur e.g. through pre-existing magnetic null points (see e.g. Roussev et al., 2007 for a detailed modeling of such a process). But it is difficult to imagine this process taking place around the whole CME. Wills-Davey and Attrill (2009) responded to the Delannée (2009) criticism by pointing out that a closed field topology is irrelevant for the reconnection with small-scale fields as the large-scale field lines become open during the CME eruption. The footpoints of these large-scale field lines are situated in the coronal dimming areas. However, coronal dimmings are usually observed behind the EIT wave front (see Fig. 4), i.e. the magnetic field of the expanding CME would encounter closed large-scale magnetic field of the quiet Sun. Even if it does encounter open large-scale field lines, it is still unclear how the CME magnetic field could go through them to produce a globally propagating EIT wave.

EUV bright fronts associated with interchange reconnection can be observed during eruptive events (Crooker and Webb, 2006; Attrill et al., 2006). But these bright fronts result from very special magnetic field topologies, when the CME magnetic field becomes adjacent to an oppositely directed open magnetic field of a coronal hole. These bright fronts are very slow and they eventually stop after propagating along a very short distance that is much smaller than global EIT wave scales (see Section 2.3).

Finally, Zhukov and Auchère (2004) suggested that different physical processes can be responsible for observed EIT wave signatures in a single event. They introduced the concept of the EIT wave bimodality on the base of morphological characteristics of two EIT wave events. The wave mode has an appearance of a propagating wave (probably a fast magnetosonic wave). The eruptive mode is exhibited as a propagation of a compressive bright front (and dimming behind it) due to the coronal magnetic field opening during the CME lift-off, e.g. in the framework of the model developed by Chen et al. (2002). Both modes can be present in the same EIT wave event, although not necessarily observed with the present instrumentation. Thus, there may be no need to look for a unique EIT wave model that can explain the variety of all the observational data.

4. EIT wave research using STEREO data

First of all, it should be mentioned that the expression "pre-STEREO" in this review does not imply a chronological association. It refers rather to the EIT wave analysis made without STEREO data. Indeed, some EIT wave studies (e.g. Chen, 2009) were made after the launch of the STEREO mission but they did not use STEREO data.

The launch of the STEREO mission (Solar TErrestrial RElations Observatory, see Kaiser et al., 2008) brought new opportunities for EIT wave studies. STEREO consists of twin spacecraft carrying identical payloads. During their orbital motion, the separation of STEREO spacecraft is gradually increasing, with one spacecraft (STEREO Ahead, or STEREO A) leading the Earth along its orbit and the other spacecraft (STEREO Behind, or STEREO B) trailing behind the Earth. STEREO thus provides us with observations of the Sun from two vantage points. EIT waves are readily observed by the extreme ultraviolet imager (EUVI), which is a part of the SECCHI instrument suite (Sun Earth Connection Coronal and Heliospheric Investigation, see Howard et al., 2008) onboard STEREO.

STEREO/SECCHI improves our observational capabilities to investigate EIT waves in several ways. EUVI data can be routinely taken at a higher cadence (typically 2.5 min) in comparison with the cadence of EIT data (typically 12 min), and with a full-Sun field of view (contrary to TRACE data). Nearly simultaneous observations in four EUVI bandpasses (171, 195, 284, 304 Å) are possible. Although high-cadence imaging of an event cannot be made in all four bandpasses simultaneously, it is however possible to observe at a cadence of 2.5 min in one bandpass, and at a cadence of 10 min in the other three bandpasses. Thus, EUVI can provide three to four images of an EIT wave front moving at a typical speed of 250 km s^{-1}, in all four bandpasses. The observations are available from two vantage points (three, if SOHO/EIT data is also included). This greatly helps to determine the overall 3D structure of the wave and its relation to the CME structure. Finally, the field of view of EUVI (up to 1.7 $R_\odot$) and that of the white-light coronagraph COR1 (from 1.4 $R_\odot$ to 4 $R_\odot$) are overlapping, thus providing us with an opportunity to observe EIT waves in a wide range of heights and by two instruments sensitive to two physically different processes.

4.1. High-cadence observations of EIT waves by SECCHI/EUVI

The EIT wave event on May 19, 2007 was observed in great detail by STEREO (Long et al., 2008; Veronig et al., 2008; Gopalswamy et al., 2009). The angular separation between the two STEREO spacecraft was 8.6°, which is too small to make a 3D reconstruction of the EIT wave structure (see Section 4.3). However, EUVI observed the wave at a cadence of 2.5 min in the 171 Å bandpass, 10 min in the 195 and 304 Å bandpasses, and 20 min in the 284 Å bandpass. High-cadence observations of the EIT wave front in the 171 Å bandpass were described by Long et al. (2008) and Veronig et al. (2008). These works reported a consistent deceleration of the wave after 12:51:30 UT. The wave speed at this instant was around 500 km s^{-1}, and the final speed 20 min later was around 180 km s^{-1}. This is the first time that the deceleration of the EIT wave was reliably measured, giving support to the interpretation of the EIT wave as a decelerating fast magnetosonic wave (e.g. Warmuth et al., 2004a). However, despite the availability of the Hα data, an associated Moreton wave was not observed (Veronig et al., 2008). Further, Ma et al. (2009) confirmed, on the basis of observations of
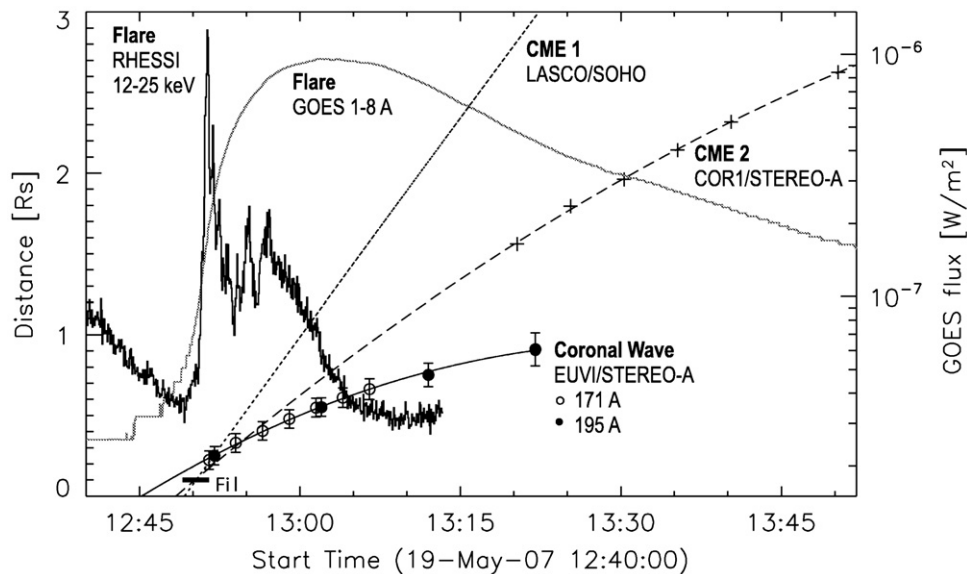
Fig. 7. Propagation of the EIT wave on May 19, 2007 measured in two SECCHI/EUVI bandpasses onboard STEREO A (circles) together with its quadratic fit. Also shown is the flare emission in soft and X-rays measured by GOES and RHESSI, respectively, and the quadratic fits of the kinematics of two associated CMEs (dashed and dotted curves). The horizontal bar shows the start of the filament eruption associated with the CME. From Veronig et al. (2008). Reproduced by permission of the AAS.

another event, that the EIT wave speed can be underestimated if a low imaging cadence is used.

It is interesting to note that Long et al. (2008) measured the wave propagation even before 12:51:30 UT. They reported that the wave was accelerating until that instant, whereas Veronig et al. (2008) did not report any measurement of the EIT wave front before 12:51:30 UT. A careful inspection of the EUVI data for this event shows that Long et al. (2008) probably measured the displacement of bright loop-like structures before 12:51:30 UT. Ma et al. (2009) and Chen et al. (2010) also mention difficulties in distinguishing the EIT wave from erupting structures early in the event.

High-cadence imaging of the EIT wave on May 19, 2007 allowed Veronig et al. (2008) to clarify the timing of the wave with respect to the associated flare observed by RHESSI (Reuven Ramaty high-energy solar spectroscopic imager, see Lin et al., 2002). The hard X-ray flux of the flare (at energies 12-25 keV) started to increase at 12:50 UT and peaked at 12:51:30 UT, when the first EIT wave front was already observed (Fig. 7). This indicates that the flare occurred too late to produce the EIT wave, since the wave requires a certain time to build up a sufficiently large amplitude to be detected in the EUVI data (Veronig et al., 2008). This fact increases the evidence that flares in general are not responsible for the EIT wave generation (see Section 2.5). It has to be noted that the flare soft X-ray flux started to grow before any noticeable increase of the hard X-ray flux, so the flare origin of the wave cannot be ruled out completely. The slow and weak increase of the flare soft X-ray flux may, however, indicate a weak energy release, too low to launch a noticeable EIT wave, see e.g. Vršnak and Cliver (2008) for a discussion on the possibility to launch a fast magnetosonic wave by a flare pressure pulse. Veronig et al. (2008) suggest that the wave is produced by the expanding CME flanks. It is driven over a limited distance and then propagates freely.

Patsourakos et al. (2009) investigated high-cadence observations of an EIT wave on December 7, 2007 and found that it was closely associated with the expanding motion of coronal loops. The blast wave produced by the flare in the core of the active region is expected to be first detected close to the flare site. Therefore, Patsourakos et al. (2009) argue in favor of the CME-driven wave hypothesis as the wave was first observed at the periphery of the active region. Warmuth et al. (2004a) reported a similar behavior of

Moreton waves.[2] The wave generated in the active region core is also expected to refract rapidly towards large heights due to the strong gradient of the fast-mode speed in this region. This seems to be contrary to what is seen in the EUVI images (Patsourakos et al., 2009).

However, not all EIT waves exhibit a simple decelerating speed profile. Ma et al. (2009) found that the EIT wave event on December 7, 2007 exhibited a nearly constant speed profile. Zhukov et al. (2009) investigated an EIT wave on December 8, 2007 and found that the initial propagation speed of the wave was around 100 km s^{-1}. Then the wave slowed down to very low speeds (around 20 km s^{-1}), and finally accelerated again to reach speeds around 200 km s^{-1}. Such a change in velocity is difficult to envisage for a freely propagating wave. Zhukov et al. (2009) suggested that such a speed profile reflected the varying speed of the CME eruption. The wave front shape was nearly circular, so even symmetric EIT waves can possibly be produced via the magnetic field restructuring during the CME lift-off. This event seems to support the field line opening mechanism by Chen et al. (2002).

A partial reflection of the EIT wave at the boundary of a coronal hole (Long et al., 2008; Gopalswamy et al., 2009) strongly indicates that the EIT wave is a true wave, at least in some events. As shown by Gopalswamy et al. (2009), the incident wave propagated at a speed of around 380 km s^{-1}, and the wave reflected in the opposite direction propagated at a speed of around 280 km s^{-1}. The waves reflected in different directions may have been superposed with the incident wave, so the measurements of their speed were not always reliable. A fast magnetosonic wave reflection at the coronal hole boundary (i.e. at the boundary of the region of higher fast-mode speed) was demonstrated in the model by Wang (2000). Another type of fast magnetosonic wave reflection—that from the chromosphere—was described in the numerical simulation by Wang et al. (2009). However, a wave reflection from the chromosphere has not yet been observed.

---

[2] It has to be noted that an alternative interpretation of this observation invokes a certain time needed to produce a large-amplitude wave due to non-linear steepening. During this time the Moreton wave is supposed to be not visible (Vršnak and Cliver, 2008). However, the dependence of the wave visibility in the EUV and Hα on the wave amplitude is presently not clear.

A possibility of a wave reflection at a coronal hole boundary was confirmed in the 3D numerical MHD simulation of the CME-driven wave developed by Schmidt and Ofman (2010). Unfortunately, they used a photospheric magnetogram with artifacts next to the region of the wave propagation. To determine the wave front positions, Schmidt and Ofman (2010) chose to show the perturbations of the plasma horizontal speed in the wave front. As the plasma horizontal speed is not directly observed by EUVI, the comparison of this simulation with observations (e.g. the EIT wave deceleration reported by Veronig et al., 2008) is difficult.

Attrill (2010) questioned the EIT wave reflection described by Gopalswamy et al. (2009) and argued that apparently reflected wave fronts result from artifacts of running difference images. However, after inspecting base difference images (that are supposed to be free from artifacts, see e.g. Wills-Davey, 2006), Attrill (2010) claimed that the EIT wave front "turned" during its propagation. This is very close to the description of a reflection, although in this case it seems more precise to speak about the refraction of the wave in the medium with an inhomogeneous Alfvén speed distribution (Uchida, 1968; Wang, 2000). Similarly, Attrill (2010) claimed that another reflected wave front moved "significantly backward". This formulation is again very close to the description of a reflection. Attrill (2010) explained the third reflected front by invoking the existence of two EIT wave fronts. Only one wave front is obvious in the EUVI data for this event (Long et al., 2008; Veronig et al., 2008; Gopalswamy et al., 2009).

It may be further argued that, in the case of a wave reflected backward to the eruption site, one should not use a pre-event image to construct base difference images. Indeed, the background intensity may have changed e.g. due to the dimming, so one needs to detect the wave propagation against a new, dimmer background. If the decrease in EUV intensity due to a dimming is significantly greater than the wave amplitude (as it is often the case), the wave would be difficult to detect in base difference images that use a pre-event image as the base image.

Veronig et al. (2010) reported the evolution of an EIT wave profile measured in the 195 Å bandpass for the eruption on January 17, 2010. The speed of the lateral expansion of the wave was approximately 280 km s^{-1}. This was significantly lower than the speed of its upward expansion that was around 650 km s^{-1}. Veronig et al. (2010) suggested two explanations for this difference. Firstly, it may be attributed to the difference in the local fast magnetosonic speed. Secondly, the wave in the upward direction may be CME-driven, so the wave speed depends on the CME speed. The lateral expansion of the wave corresponds to a free propagation during most of the time in both cases. Its speed is determined by the local plasma and magnetic field parameters.

Veronig et al. (2010) showed that the wave profile was first steepening and the wave amplitude was growing. Further on, the amplitude was decreasing steadily and the wave profile width was increasing, with the integral below the profile remaining approximately constant. This behavior is consistent with the 3D evolution of a non-linear fast magnetosonic wave (e.g. Landau and Lifshitz, 1987). According to Veronig et al. (2010), the wave is first driven by the CME lateral expansion. Shortly afterward, the CME expansion stops. Evidence for this is given by the limited extent of the associated coronal dimmings compared to the global distances traveled by the wave. After the end of the driven phase, the wave is propagating freely in the lateral direction.

Yang and Chen (2010) investigated two EIT wave events observed by SECCHI/EUVI. They found a negative correlation between the EIT wave speed and the coronal magnetic field calculated using the PFSS model. This means that EIT waves propagate faster in regions with a low magnetic field. If the EIT wave is a coronal fast magnetosonic wave, then a positive correlation would be expected, as can be seen from Eq. (1), although such a comparison neglects the dependence of the fast magnetosonic speed on density. Yang and Chen (2010) argued that the negative correlation can be explained by the field line opening model by Chen et al. (2002), although this explanation strongly depends on the adopted configuration of the coronal magnetic field. It also needs to be noted that Yang and Chen (2010) measured the wave propagation close to the wave source, where the wave may be driven rather than freely propagating.

The high cadence of SECCHI/EUVI enabled a detailed imaging of the May 19, 2007 event that could be compared with spectroscopic observations made by Hinode/EIS, as reported by Chen et al. (2010). The EIT wave rapidly passed along the spectrometer slit, and it was difficult to distinguish from the movement of pre-existing loop structures. The wave front was not very clear, but it seemed to be better observed in the Fe XIII (202.04 Å) line intensity than in the Fe XII (195.12 Å) line intensity. The EIT wave was not detected in Doppler velocity measurements or in the spectral line width, which is in agreement with previous results by Harra and Sterling (2001, 2003). Strong outflows in the dimming region behind the EIT wave front and increased line widths can be explained using the field line opening model by Chen et al. (2002). Chen et al. (2010) argued that the absence of spectral signatures of the wave front is also compatible with the fast magnetosonic wave model. Indeed, the velocity perturbation in the fast magnetosonic wave front would be directed across the line of sight for a wave front observed near the disc center.

High-cadence observations of small-scale bright fronts similar to large-scale EIT waves were reported by Podladchikova et al. (2010). They proposed an interpretation of these small-scale fronts in terms of slow-mode MHD waves propagating nearly perpendicularly to the ambient magnetic field. It should be noted that speeds reported by Podladchikova et al. (2010) are around 14 km s^{-1}. This value is an order of magnitude lower than typical EIT wave speeds of approximately 250 km s^{-1}.

4.2. Simultaneous observations of EIT waves in several SECCHI/EUVI bandpasses

Long et al. (2008) investigated the EIT wave on May 19, 2007 and demonstrated that the wave was cospatial in all four EUVI bandpasses (Fig. 8). These observations thus confirm earlier results on the EIT wave visibility in the 171 and 284 Å bandpasses by Wills-Davey and Thompson (1999) and Zhukov and Auchère (2004), respectively. The EIT wave detection in the 304 Å bandpass was reported by Long et al. (2008) for the first time. The wave front contrast was strongest in the 195 Å bandpass and weakest in the 304 Å bandpass. Although the 304 Å bandpass is dominated by the He II line at 303.78 Å formed in the upper transition region (peak formation temperature around 0.08 MK), it is most probable that the EIT wave radiation was detected in the Si XI line at 303.324 Å, that is formed in the corona at temperatures around 1.6 MK (Long et al., 2008).

The EIT wave visibility in three coronal EUVI bandpasses was confirmed by Attrill et al. (2009) who also reported the EIT wave detection in the soft X-ray data taken by XRT (X-ray telescope, see Golub et al., 2007) onboard Hinode. It has to be mentioned that Hinode/XRT is more sensitive to temperatures around 1-2 MK than Yohkoh/SXT. Patsourakos et al. (2009) confirmed that EIT waves are most visible at temperatures between 1 and 2 MK that are close to the peak of the quiet Sun differential emission measure $d\psi/dT$ (see e.g. Brosius et al., 1996). Patsourakos et al. (2009) suggest that the visibility of the EIT wave in several bandpasses and its strongest contrast at these temperatures demonstrate that the EIT waves represent a density increase rather than a temperature change.
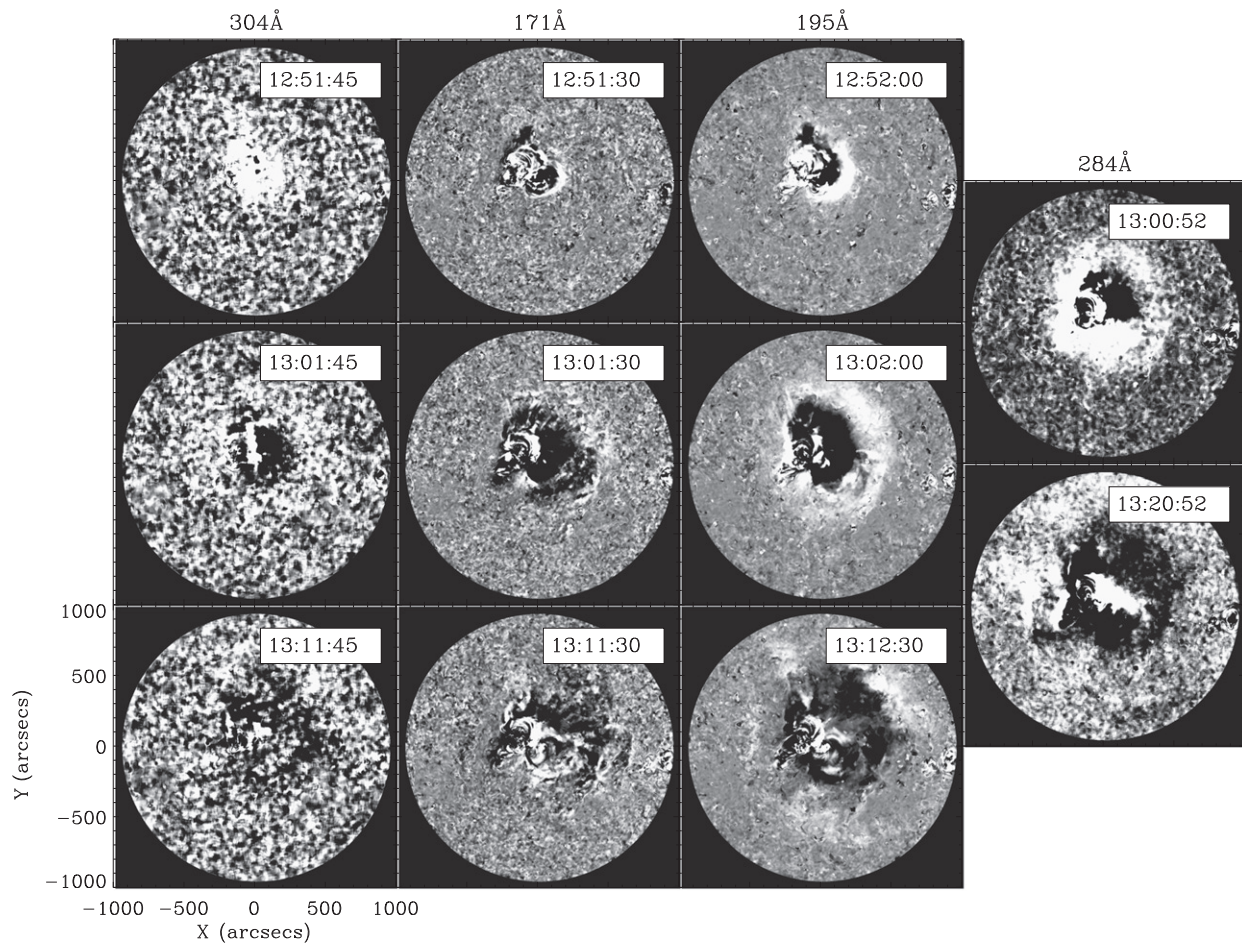
Fig. 8. EIT wave on May 19, 2007 observed in four bandpasses of SECCHI/EUVI onboard STEREO A. All images are running difference images. A boxcar filter was applied to each image (Long et al., 2008) in order to improve the visibility of the faint wave structures. From Long et al. (2008). Reproduced by permission of the AAS.

In the event reported by Attrill et al. (2009), some parts of the wave front had stronger contrast in the 284 Å bandpass than in the 195 Å bandpass. Moreover, the brightest part of the front seen in 284 and 195 Å bandpasses had no detectable counterpart in the 171 Å bandpass. Dai et al. (2010) investigated the EIT wave event on December 31, 2007 that was observed in three coronal EUVI bandpasses and also concluded that the EIT wave appeared dark in the 171 Å bandpass. These observations favor the heating of the coronal plasma up to 1.4 MK (peak formation temperature of the Fe XII line at 195 Å) rather than the plasma compression as the main factor producing the observed intensity change in the 171 and 195 Å bandpasses.

Veronig et al. (2010) compared the wave contrast measured in three coronal EUVI bandpasses. They found that the EIT wave contrast is strongest in the 195 Å bandpass and weakest in the 171 Å bandpass. This indicates that the temperature changes in the EIT wave fronts as well as density, thus confirming earlier results reported by Wills-Davey and Thompson (1999).

4.3. Three-dimensional structure of EIT waves

In this section, the issue of the 3D structure of EIT waves will be addressed, together with a closely linked question of the relation between EIT waves and the CME structure.

Three-dimensional reconstruction of coronal loops, promi-nences and other small-scale structures in the solar atmosphere requires imaging from two vantage points that are not very much

separated from each other (e.g. Inhester, 2006; Feng et al., 2007; Gissot et al., 2008; Aschwanden et al., 2008; Rodriguez et al., 2009), typically below 15°. On the contrary, 3D reconstruction of large-scale optically thin structures (like EIT waves) requires a larger angular separation between the two vantage points.

Patsourakos et al. (2009) and Ma et al. (2009) investigated the EIT wave event on December 7, 2007 that was observed from two STEREO spacecraft separated by around 45°. Both works reported a difference in the EIT wave appearance as seen from two spacecraft early in the event. Namely, the brightest part of the EIT wave was situated to the east (west) of the source active region in the STEREO A (STEREO B) data. Ma et al. (2009) found that, in spite of correction for projection effects on the solar disk, the EIT wave speeds as measured by STEREO A and B spacecraft were different. The different appearance of wave fronts in STEREO A and B observations is a result of a different emission measures being integrated along different lines of sight (Fig. 9). This indicates that the EIT wave front extends over a non-negligible height range, and the full 3D structure of the EIT wave must be taken into account to measure its kinematics. Patsourakos et al. (2009) made a first attempt to determine the EIT wave height in this event. They used a geometric triangulation of the wave front as observed from two vantage points and obtained a wave height of around 90 mm. The fact that they reported no height range, stresses the difficulties in deriving the 3D structure of a diffuse optically thin object.

Patsourakos et al. (2009) fitted the CME associated with this EIT wave with a geometrical flux rope model (Thernisien et al., 2006, see also Chen et al., 2000). The flux rope was then projected on the
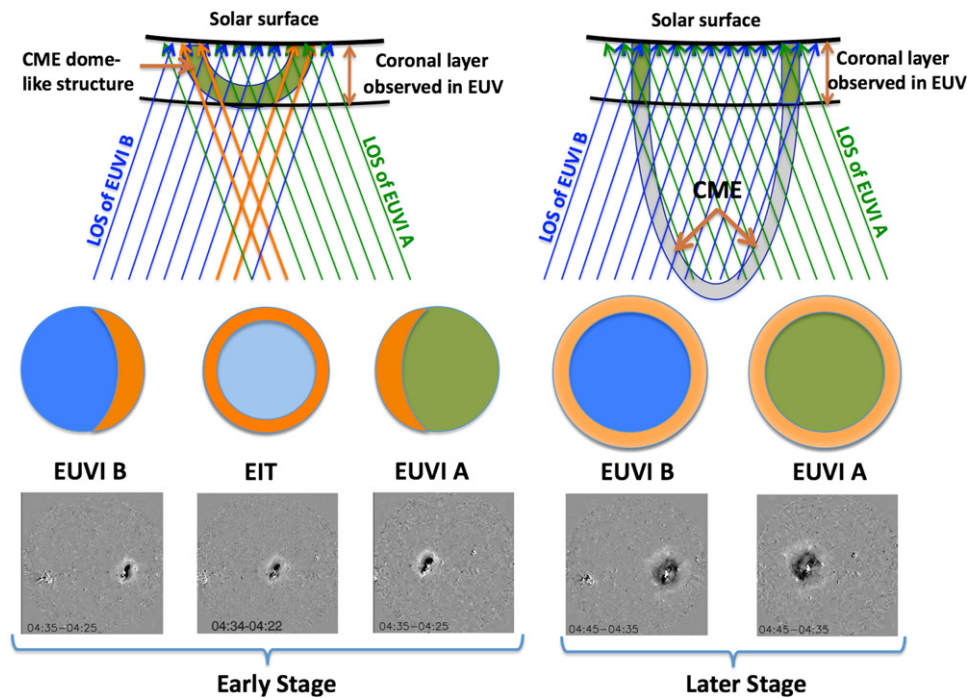
Fig. 9. A cartoon illustrating the projection effect on the EIT wave observations from several viewpoints. In the early stages, the observed EIT wave front structure is different depending on the vantage point (STEREO B, SOHO and STEREO A). The different appearance is due to different emission measures integrated along three different lines of sight. The orange-colored regions schematically represent positions of high-intensity regions along the EIT wave front. Images of the EIT wave on December 7, 2007 are shown in the bottom row for comparison. Note that the dome-like structure shown in the figure may not represent a CME, but a true wave, e.g. a CME-driven fast magnetosonic wave. The EIT wave appearance would be the same in both cases. From Ma et al. (2009). Reproduced by permission of the AAS.

solar disc to simulate the EIT wave appearance as if it would be generated by non-wave models like those of Delannée et al. (2008) or Chen et al. (2002). Patsourakos et al. (2009) argued that the flux rope projections did not resemble the observed EIT wave appearance. However, the flux rope model by Thernisien et al. (2006) was designed to reproduce structured CMEs (e.g. Cremades and Bothmer, 2004). On the contrary, the CME observed by COR1 in association with this EIT wave event is very diffuse and its overall structure is not at all clear.

On the contrary, Ma et al. (2009) found that the different appearance of the wave as seen from two STEREO spacecraft during the early propagation stage is consistent with the projection of the CME dome-like structure (Fig. 9). However, this dome-shaped structure can represent a large-scale fast magnetosonic wave equally well. Additionally, the footpoints of this dome-shaped structure are fixed to the solar surface, contrary to the observations of the EIT wave propagating to large distances from the source active region.

Zhukov and Auchère (2004) suggested that STEREO observations from widely separated vantage points should be used to study the link between EIT waves and the CME structure. Indeed, the EIT wave is best seen on-disk and the overlying CME structure is best seen above the limb. Patsourakos and Vourlidas (2009) investigated the EIT wave event on February 13, 2009 that was observed by the STEREO spacecraft in quadrature (angular separation around 90°). Images of this event taken by EUVI onboard STEREO A and B in the 195 Å bandpass are shown in Fig. 10.

It is clear that the wave is observed over a range of heights from the solar surface to around 100 mm. Patsourakos and Vourlidas (2009) reported that the lateral extent of the EIT wave as observed by EUVI was significantly wider than the CME lateral extent as measured in the EUVI and COR1 data. SECCHI data thus confirm a general tendency that an EIT wave is often global, but

corresponding coronal dimmings (that map to the footpoints of the associated CME) are usually localized (e.g. Dere et al., 1997a; Sterling and Hudson, 1997; Thompson et al., 1998, 2000a; Zhukov and Auchère, 2004). In addition, oscillations of quasi-radial structures in the quiet Sun were observed after the EIT wave passage (similar to the loop oscillations reported by Wills-Davey and Thompson, 1999). These two facts suggest that, at least in this event, the EIT wave is not linked to the magnetic field restructuring but is rather a fast magnetosonic wave. The same conclusion was reached by Kienreich et al. (2009) who investigated only the EUVI data and suggested that the wave was initially driven by the CME lateral expansion and later propagated freely.

However, the conclusion of a similar study made using the data taken by EIT and by the MK3 coronagraph was very different: the EIT wave was co-spatial with the legs of the CME frontal loop (Chen, 2009). Two other EIT wave events observed by EUVI and COR1 provide us with evidence that the EIT wave propagation matched the lateral expansion of the outer boundary of the CME (Attrill et al., 2009; Dai et al., 2010). These two works conclude that the EIT wave is not a true wave, but is rather produced by the magnetic field reconfiguration during the CME lift-off.

An alternative interpretation of the February 13, 2009 event was presented by Cohen et al. (2009) who performed a 3D numerical MHD simulation of the CME and EIT wave. A flux rope was inserted in a realistic configuration of coronal plasma and magnetic field. The flux rope was set to erupt at a speed similar to the observed CME speed. An EIT wave was seen in the simulated images as a density perturbation. Cohen et al. (2009) found that the EIT wave was a combination of both true wave and non-wave mechanisms, that is similar to the EIT wave bimodality suggested by Zhukov and Auchère (2004). The EIT wave front was found to match the position of the outer surface of the CME. Cohen et al. (2009) argued that the non-wave component of the EIT wave front is produced by
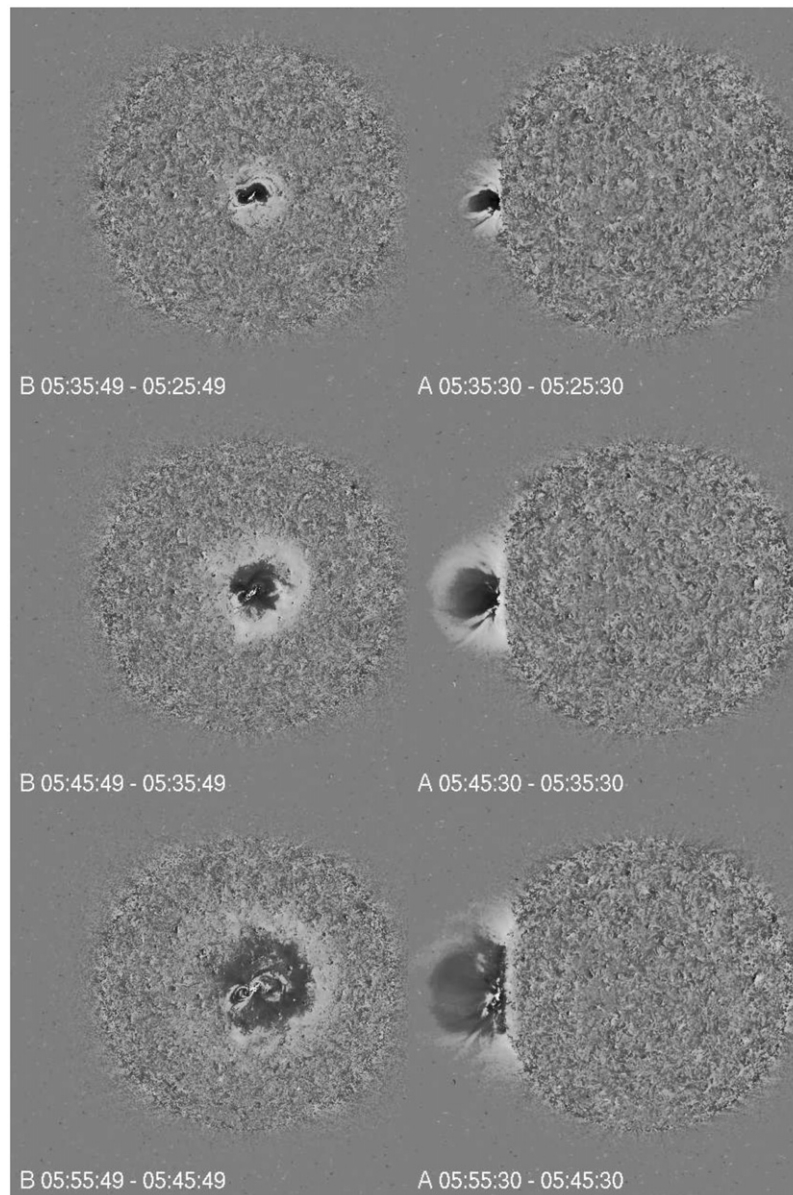
Fig. 10. EIT wave on February 13, 2009 as observed by SECCHI/EUVI onboard STEREO B (left column) and STEREO A (right column) in the Fe XII (195 Å) bandpass. All images are running difference images. The angular separation of the two STEREO spacecraft was around 90° (quadrature configuration). Note that the time stamps of images taken by the two spacecraft are different to account for the difference in the light travel time from the Sun to each STEREO spacecraft. The event on the Sun is thus observed by the two spacecraft simultaneously. All times are UT.

the reconnection of the erupting flux rope with the ambient large-scale magnetic field (see also Cohen et al., 2010). It has to be noted that this conclusion looks different from the idea proposed by Attrill et al. (2007) who considered reconnection with small-scale quiet Sun magnetic fields.

However, although the reconnection of the flux rope with the ambient field is clearly shown in this simulation, it occurs only in one place—to the north of the erupting active region (see Figures 7 and 8 in the paper by Cohen et al., 2009)—where the orientations of magnetic fields in the CME and in the ambient corona are nearly opposite and thus favorable for reconnection. This process then can hardly produce a quasi-circular wave front. The reconnection in the EIT wave front reported by Cohen et al. (2009) is similar to interchange reconnection between the erupting and ambient magnetic fields (Crooker and Webb, 2006; Attrill et al., 2006; Gibson and Fan, 2008). The interchange reconnection also results in a CME that becomes much wider than the CME observed by SECCHI.

In the movie supplied with the Cohen et al. (2009) paper, it can be seen that at 07:05 UT the observed CME width is around 60° whereas the simulation shows the CME width of around 120°.

There also exists a question regarding the nature of the true wave component in the simulation by Cohen et al. (2009). The CME-driven shock is situated much ahead of the EIT wave front. However, the CME-driven shock should be visible not only as a temperature increase (as in Figure 9 of the paper by Cohen et al., 2009), but also as a density increase. This is not the case in the simulation by Cohen et al. (2009).

4.4. Summary of EIT wave observations made by STEREO

Observations by SECCHI/EUVI onboard STEREO significantly advanced our understanding of the EIT wave phenomenon. High-cadence EUVI data confirm the possibility of the EIT wave

deceleration (Veronig et al., 2008; Long et al., 2008), although constant velocities (Ma et al., 2009) and more complicated speed profiles (Zhukov et al., 2009) are observed as well. The evolution of the wave profile is consistent with the wave first driven by the CME expanding flanks, and then propagating freely (Veronig et al., 2010). The EIT wave reflection at the coronal hole boundary (Long et al., 2008; Gopalswamy et al., 2009) provides us with strong evidence that the EIT wave is a true wave, at least in the reported event. The data taken in several EUV bandpasses show the multi-temperature structure of EIT waves (Attrill et al., 2009; Dai et al., 2010; Veronig et al., 2010). It was demonstrated that some EIT waves are compressive disturbances (Long et al., 2008; Patsourakos et al., 2009), but the plasma heating can be observed in EIT wave fronts as well (Attrill et al., 2009; Dai et al., 2010). A slower EIT wave propagation in stronger coronal magnetic fields was reported for two events (Yang and Chen, 2010), indicating a difficulty to explain them by the fast magnetosonic wave model. Finally, the interpretations of the 3D structure of EIT waves and their relation to the associated CME structures are often contradictory, with different authors favoring true wave (Patsourakos et al., 2009; Patsourakos and Vourlidas, 2009; Kienreich et al., 2009), non-wave (Ma et al., 2009; Yang and Chen, 2010) and bimodal (Cohen et al., 2009) hypotheses of the EIT wave origin. STEREO observations show that the wave is a continuous front extending from the solar surface up to around 100 mm. Therefore, STEREO data do not favor the electric current shell model of Delannée et al. (2008) that predicts the EIT wave emission coming from high in the corona.

5. Discussion

5.1. Terminological issue

Different names exist in the literature for the solar phenomenon discussed in this paper: EIT wave (e.g. Delannée, 2000; Thompson and Myers, 2009), coronal Moreton wave (e.g. Thompson et al., 1999), flare wave (e.g. Warmuth et al., 2004a), coronal wave (Attrill et al., 2007), EUV wave (Patsourakos and Vourlidas, 2009), coronal bright front (Gallagher and Long, 2010). "Flare wave" implies a close relation to flares, but, as it was demonstrated in Section 2.5, the phenomenon shows a better correlation with CMEs. The term "coronal Moreton wave" also implies an unambiguous association with Moreton waves, although EIT waves are observed much more frequently than Moreton waves, and their relation is still not clear. The terms "coronal wave" and "EUV wave" may lead to a confusion with other waves observed in the EUV corona, e.g. with slow magnetosonic waves in loops and plumes (Deforest and Gurman, 1998; Berghmans and Clette, 1999; De Moortel et al., 2000; Robbrecht et al., 2001). The term "coronal bright front" recently suggested by Gallagher and Long (2010) has an advantage that it does not imply any physical mechanism. Indeed, some of these fronts may be not waves at all (see Section 3). However, the meaning of this term is too wide. For example, a CME frontal loop observed by a coronagraph can also be called a coronal bright front. The term "EIT wave" is preferred in this review. It only signifies that the phenomenon was discovered in the EIT data. Similarly, the term "Moreton wave" signifies that the phenomenon was discovered by Moreton (1960). The term "EIT wave" by no means implies that the "EIT wave" phenomenon can be only observed by the EIT telescope.

5.2. Prospects for future research

On the observational side, EIT wave research is still hampered by insufficient knowledge of plasma and magnetic field parameters in the solar atmosphere. The works by Uchida (1968) and Wang (2000) demonstrate the importance of the coronal Alfvén speed distribution for the propagation of EIT and Moreton waves. Spectroscopic observations are necessary for better plasma diagnostics in EIT wave fronts and in the ambient corona. The work by Asai et al. (2008) is an important step in this direction, and physical interpretation and modeling of spectroscopic EIS data need to be performed.

On the theoretical side, one can distinguish two directions for EIT wave modeling, depending on the spatial scale described by a model. Firstly, the properties of a global-scale EIT wave propagation in a realistic model atmosphere need to be fully and consistently described. Secondly, the small-scale structure and evolution of EIT wave fronts in the corona need to be modeled.

Regarding the modeling of global-scale propagation, the relation between Moreton and EIT waves is still unclear. In many cases it looks like these are two different manifestations of a single propagating fast magnetosonic wave (e.g. Warmuth et al., 2001; Warmuth, 2007). The compression in the coronal part of the fast magnetosonic wave is then seen as an EIT wave.[3] However, the conditions for the appearance of the Moreton wave are still unknown. It was suggested (see e.g. Wang, 2000) that the Moreton wave is a strongly supermagnetosonic wave or shock (with Alfvén-Mach number $M_A > 1$). As it propagates further on from the erupting active region, its amplitude decreases and only the EIT wave ($M_A \sim 1$) is visible. In this case the models by Uchida (1968) and Wang (2000) cannot be used as they both assume a weak perturbation propagating all the time at the fast magnetosonic speed v_f (i.e. a linear regime with $M_A \sim 1$). The rapid dissipation expected for such a strong supermagnetosonic shock (Uchida, 1968) has not been modeled yet. A model of the fast MHD shock propagation in realistic coronal conditions and its decay into a non-shocked wave needs to be developed to answer this question.

The interaction of a fast magnetosonic wave with the chromosphere (e.g. Gilbert and Holzer, 2004) should be modeled to derive the quantitative criterion required for a Moreton wave to be detected. One also needs to determine if there is a limiting value of M_A (or the wave amplitude) below which the Moreton wave cannot be observed. It is still not clear if a different distribution of the coronal Alfvén speed (e.g. Evans et al., 2008) may explain the appearance (or not) of Moreton waves in different events. It has to be noted that in the case of a strongly non-linear perturbation (e.g. a blast wave) the wave propagation is not sensitive to the distribution of the ambient Alfvén speed (Sedov, 1959; Zel'dovich and Raizer, 1967; Landau and Lifshitz, 1987). The narrow angular span of Moreton waves in contrast to the quasi-circular EIT wave fronts has not yet been modeled either.

However, in some events EIT and Moreton waves probably represent two different disturbances (Eto et al., 2002). The Moreton wave is then still a fast magnetosonic wave (no other model has been suggested so far), and probably CME-produced. The EIT wave should then be generated by some other mechanism, possibly related to the coronal magnetic field restructuring during the CME lift-off (e.g. Chen et al., 2002; Pomoell et al., 2008). The development of 3D models in the framework of this interesting mechanism is necessary.

No Moreton wave observations have been reported after the launch of STEREO. The separation of the two STEREO spacecraft is currently very large for the EUVI data to be reliably compared with Hα observations from ground-based observatories. High-cadence EUV data for comparison with Hα data can be provided by the Atmospheric Imaging Assembly (AIA, see Title, 2006) onboard the Solar Dynamics Observatory (SDO). The resulting detailed observations need to be accordingly modeled.

---

[3] Note that the inverse may not necessarily be true: not every EIT wave is an observed manifestation of a fast magnetosonic wave.

Regarding the modeling of EIT wave fronts on a smaller scale, the structure and evolution of the EIT wave perturbation need to be addressed in detail. A non-linear theoretical treatment of MHD waves (see e.g. a review by Polovin, 1961) shows that, in a case of weak dispersion, the fast magnetosonic wave profile should steepen and eventually result in a discontinuity (shock wave). An analogous behavior of non-linear waves can be found in hydrodynamics (e.g. Landau and Lifshitz, 1987). The increase of the EIT wave amplitude and the steepening of its profile were reported by Veronig et al. (2010) in high-cadence EUVI data, although this behavior was visible only in two images. In addition, the propagation speed of a non-linear fast magnetosonic wave should increase with increasing wave amplitude. This acceleration has not yet been observed.

An application of non-linear MHD wave modeling to coronal shock waves manifested by type II radio bursts was developed by Vršnak and Lulić (2000a,b) for a 1D geometry, and by Žic et al. (2008) for a 3D geometry. These models have not yet been applied to EIT wave observations. It has to be noted that in the 3D spherical geometry, the steepening of the wave profile is more difficult to achieve in a dissipative medium, as the wave amplitude decreases with distance due to the conservation of energy (Landau and Lifshitz, 1987). In the presence of dispersion, a soliton-like solution may be applicable (Wills-Davey et al., 2007).

Due to limited EIT cadence, the EIT wave models (e.g. Wang, 2000; Wu et al., 2001; Chen et al., 2002; Delannée et al., 2008) were rather developed to explain their global propagation. Measurements of the wave profile evolution are more difficult (Wills-Davey, 2006), and only after the launch of the STEREO mission the situation somewhat improved (Veronig et al., 2010). Routine measurements of the EIT wave profile evolution will be made with high-cadence, high-resolution SDO/AIA data. These observations will be compared with results of non-linear MHD wave theory. A complicated temperature structure of the EIT wave front (e.g. Wills-Davey and Thompson, 1999) and the wave propagation in the structured corona (see Murawski et al., 2001) need to be addressed.

Non-wave modeling of the EIT wave perturbation is still somewhat lagging behind the true wave modeling. This is primarily due to the extensive literature on MHD waves accumulated during the last 60 years. In particular, it is still unclear if compression produced by the field line opening mechanism (Chen et al., 2002; Pomoell et al., 2008) is sufficient to explain the observed density increase in EIT wave fronts and its evolution during the wave propagation.

EIT waves exhibit a wide range of observational characteristics, especially regarding their morphology and speed. Namely, EIT wave propagation speed can vary greatly between different events. It can be both higher and lower than the coronal sound speed. This fact makes an exclusive interpretation of EIT waves in terms of either a fast or slow magnetosonic wave unlikely. It is hard to believe that all EIT waves could be explained by a single physical mechanism, wave or non-wave model regardless. Biesecker et al. (2002) suggested that several types of EIT waves may exist. Namely, they argue that narrow S-waves may represent a physically distinct class of phenomena. We note that the evolution of S-waves is not clear due to insufficient cadence of images taken by SOHO/EIT. No S-waves have yet been reported in the improved STEREO observations. Developing further the idea by Biesecker et al. (2002), Zhukov and Auchère (2004) introduced a concept of EIT wave bimodality. This means that both wave and non-wave physical mechanisms can be at work in the same event, although not necessarily detected with the current instrumentation. In order to determine what mechanisms are important in each specific EIT wave event, a quantitative modeling of EIT wave front parameters is now essential. Three-dimensional models using realistic values of coronal plasma and magnetic field parameters that are capable of

simulating the observed EUV emission (e.g. Linker et al., 2008) are needed.

6. Conclusions

The EIT wave phenomenon is still far from being completely understood. No single model can account for a large variety of observed properties of EIT waves. It is mainly theoretical and modeling efforts, as well as spectroscopic diagnostics, that are required to advance our understanding of this complex phenomenon. The theoretical progress will probably be linked to the development of advanced models capable of simulating observable parameters. Comparison of quantitative models with recent and upcoming observational data (taken by SOHO, Hinode, STEREO, SDO) can then be performed to determine the relative importance of different physical mechanisms contributing to the observational "EIT wave" phenomenon.

References

Arnaud, M., Raymond, J., 1992. Iron ionization and recombination rates and ionization equilibrium. Astrophys. J. 398, 394–406.

Asai, A., Hara, H., Watanabe, T., Imada, S., Sakao, T., Narukage, N., Culhane, J.L., Doschek, G.A., 2008. Strongly blueshifted phenomena observed with hinode EIS in the 2006 December 13 solar flare. Astrophys. J. 685, 622–628.

Aschwanden, M.J., Schrijver, C.J., Alexander, D., 2001. Modeling of coronal EUV loops observed with TRACE. I. Hydrostatic solutions with nonuniform heating. Astrophys. J. 550, 1036–1050.

Aschwanden, M.J., Wülser, J., Nitta, N.V., Lemen, J.R., 2008. First three-dimensional reconstructions of coronal loops with the STEREO A and B spacecraft. I. Geometry. Astrophys. J. 679, 827–842.

Athay, R.G., Moreton, G.E., 1961. Impulsive phenomena of the solar atmosphere. I. Some optical events associated with flares showing explosive phase. Astrophys. J. 133, 935–945.

Attrill, G., Nakwacki, M.S., Harra, L.K., van Driel-Gesztelyi, L., Mandrini, C.H., Dasso, S., Wang, J., 2006. Using the evolution of coronal dimming regions to probe the global magnetic field topology. Sol. Phys. 238, 117–139.

Attrill, G.D.R., 2010. Dispelling illusions of reflection: a new analysis of the 2007 May 19 coronal "wave" event. Astrophys. J. 718, 494–501.

Attrill, G.D.R., Engell, A.J., Wills-Davey, M.J., Grigis, P., Testa, P., 2009. Hinode/XRT and STEREO observations of a diffuse coronal "wave"-coronal mass ejection-dimming event. Astrophys. J. 704, 1296–1308.

Attrill, G.D.R., Harra, L.K., van Driel-Gesztelyi, L., Démoulin, P., 2007. Coronal "wave": magnetic footprint of a coronal mass ejection? Astrophys. J. 656, L101–L104.

Ballai, I., Erdélyi, R., Pintér, B., 2005. On the nature of coronal EIT waves. Astrophys. J. 633, L145–L148.

Berghmans, D., Clette, F., 1999. Active region EUV transient brightenings—first results by EIT of SOHO JOP80. Sol. Phys. 186, 207–229.

Biesecker, D.A., Myers, D.C., Thompson, B.J., Hammer, D.M., Vourlidas, A., 2002. Solar phenomena associated with "EIT waves". Astrophys. J. 569, 1009–1015.

Blokhintsev, D.I., 1981. Acoustics of Nonhomogeneous Moving Medium. Nauka, Moscow.

Brosius, J.W., Davila, J.M., Thomas, R.J., Monsignori-Fossi, B.C., 1996. Measuring active and quiet-sun coronal plasma properties with extreme-ultraviolet spectra from SERTS. Astrophys. J. Suppl. Ser. 106, 143–164.

Brueckner, G.E., Howard, R.A., Koomen, M.J., Korendyke, C.M., Michels, D.J., Moses, J.D., Socker, D.G., Dere, K.P., Lamy, P.L., Llebaria, A., Bout, M.V., Schwenn, R., Simnett, G.M., Bedford, D.K., Eyles, C.J., 1995. The large angle spectroscopic coronagraph (LASCO). Sol. Phys. 162, 357–402.

Chen, F., Ding, M.D., Chen, P.F., 2010. Spectroscopic analysis of an EIT wave/dimming observed by Hinode/EIS. Astrophys. J. 720, 1254–1261.

Chen, J., Santoro, R.A., Krall, J., Howard, R.A., Duffin, R., Moses, J.D., Brueckner, G.E., Darnell, J.A., Burkepile, J.T., 2000. Magnetic geometry and dynamics of the fast coronal mass ejection of 1997 September 9. Astrophys. J. 533, 481–500.

Chen, P.F., 2006. The relation between EIT waves and solar flares. Astrophys. J. 641, L153–L156.

Chen, P.F., 2009. The relation between EIT waves and coronal mass ejections. Astrophys. J. 698, L112–L115.

Chen, P.F., Ding, M.D., Fang, C., 2005a. Synthesis of CME-associated Moreton and EIT wave from features MHD simulations. Space Sci. Rev. 121, 201–211.

Chen, P.F., Fang, C., Shibata, K., 2005b. A full view of EIT waves. Astrophys. J. 622, 1202–1210.

Chen, P.F., Wu, S.T., Shibata, K., Fang, C., 2002. Evidence of EIT and Moreton waves in numerical simulations. Astrophys. J. 572, L99–L102.

Ciaravella, A., Raymond, J.C., Kahler, S.W., Vourlidas, A., Li, J., 2005. Detection and diagnostics of a coronal shock wave driven by a partial-halo coronal mass ejection on 2000 June 28. Astrophys. J. 621, 1121–1128.

Cliver, E.W., Laurenza, M., Storini, M., Thompson, B.J., 2005. On the origins of solar EIT waves. Astrophys. J. 631, 604–611.

Cohen, O., Attrill, G.D.R., Manchester, W.B., Wills-Davey, M.J., 2009. Numerical simulation of an EUV coronal wave based on the 2009 February 13 CME event observed by STEREO. Astrophys. J. 705, 587–602.

Cohen, O., Attrill, G.D.R., Schwadron, N.A., Crooker, N.U., Owens, M.J., Downs, C., Gombosi, T.I., 2010. Numerical simulation of the 12 May 1997 CME event: the role of magnetic reconnection. J. Geophys. Res. 115, A10104.

Cremades, H., Bothmer, V., 2004. On the three-dimensional configuration of coronal mass ejections. Astron. Astrophys. 422, 307–322.

Crooker, N.U., Webb, D.F., 2006. Remote sensing of the solar site of interchange reconnection associated with the May 1997 magnetic cloud. J. Geophys. Res. 111, A08108.

Culhane, J.L., Harra, L.K., James, A.M., Al-Janabi, K., Bradley, L.J., Chaudry, R.A., Rees, K., Tandy, J.A., Thomas, P., Whillock, M.C.R., Winter, B., Doschek, G.A., Korendyke, C.M., Brown, C.M., Myers, S., Mariska, J., Seely, J., Lang, J., Kent, B.J., Shaughnessy, B.M., Young, P.R., Simnett, G.M., Castelli, C.M., Mahmoud, S., Mapson-Menard, H., Probyn, B.J., Thomas, R.J., Davila, J., Dere, K., Windt, D., Shea, J., Hagood, R., Moye, R., Hara, H., Watanabe, T., Matsuzaki, K., Kosugi, T., Hansteen, V., Wikstol, Ø., 2007. The EUV imaging spectrometer for Hinode. Sol. Phys. 243, 19–61.

Dai, Y., Auchère, F., Vial, J., Tang, Y.H., Zong, W.G., 2010. Large-scale extreme-ultraviolet disturbances associated with a limb coronal mass ejection. Astrophys. J. 708, 913–919.

De Moortel, I., Ireland, J., Walsh, R.W., 2000. Observation of oscillations in coronal loops. Astron. Astrophys. 355, L23–L26.

Deforest, C.E., Gurman, J.B., 1998. Observation of quasi-periodic compressive waves in solar polar plumes. Astrophys. J. 501, L217–L220.

Del Zanna, G., Bromage, B.J.I., Mason, H.E., 2003. Spectroscopic characteristics of polar plumes. Astron. Astrophys. 398, 743–761.

Delaboudinière, J.P., Artzner, G.E., Brunaud, J., Gabriel, A.H., Hochedez, J.F., Millier, F., Song, X.Y., Au, B., Dere, K.P., Howard, R.A., Kreplin, R., Michels, D.J., Moses, J.D., Defise, J.M., Jamar, C., Rochus, P., Chauvineau, J.P., Marioge, J.P., Catura, R.C., Lemen, J.R., Shing, L., Stern, R.A., Gurman, J.B., Neupert, W.M., Maucherat, A., Clette, F., Cugnon, P., van Dessel, E.L., 1995. EIT: extreme-ultraviolet imaging telescope for the SOHO mission. Sol. Phys. 162, 291–312.

Delannée, C., Aulanier, G., 1999. Cme associated with transequatorial loops and a bald patch flare. Sol. Phys. 190, 107–129.

Delannée, C., 2000. Another view of the EIT wave phenomenon. Astrophys. J. 545, 512–523.

Delannée, C., 2009. The role of small versus large scale magnetic topologies in global waves. Astron. Astrophys. 495, 571–575.

Delannée, C., Delaboudinière, J.P., Lamy, P., 2000. Observation of the origin of CMEs in the low corona. Astron. Astrophys. 355, 725–742.

Delannée, C., Hochedez, J., Aulanier, G., 2007. Stationary parts of an EIT and Moreton wave: a topological model. Astron. Astrophys. 465, 603–612.

Delannée, C., Török, T., Aulanier, G., Hochedez, J., 2008. A new model for propagating parts of EIT waves: a current shell in a CME. Sol. Phys. 247, 123–150.

Dere, K.P., Brueckner, G.E., Howard, R.A., Koomen, M.J., Korendyke, C.M., Kreplin, R.W., Michels, D.J., Moses, J.D., Moulton, N.E., Socker, D.G., St. Cyr, O.C., Delaboudinière, J.P., Artzner, G.E., Brunaud, J., Gabriel, A.H., Hochedez, J.F., Millier, F., Song, X.Y., Chauvineau, J.P., Marioge, J.P., Defise, J.M., Jamar, C., Rochus, P., Catura, R.C., Lemen, J.R., Gurman, J.B., Neupert, W., Clette, F., Cugnon, P., vanDessel, E.L., Lamy, P.L., Llebaria, A., Schwenn, R., Simnett, G.M., 1997a. EIT and LASCO observations of the initiation of a coronal mass ejection. Sol. Phys. 175, 601–612.

Dere, K.P., Landi, E., Mason, H.E., Monsignori Fossi, B.C., Young, P.R., 1997b. CHIANTI—an atomic database for emission lines. Astron. Astrophys. Suppl. 125, 149–173.

Dere, K.P., Landi, E., Young, P.R., Del Zanna, G., Landini, M., Mason, H.E., 2009. CHIANTI—an atomic database for emission lines. IX. Ionization rates, recombination rates, ionization equilibria for the elements hydrogen through zinc and updated atomic data. Astron. Astrophys. 498, 915–929.

Dodson, H.W., Hedeman, E.R., 1964. Moving material accompanying the flare of 1959 July $16^d21^h14^m$ UT. NASA Spec. Publ. 50, 15–23.

Dryer, M., 1982. Coronal transient phenomena. Space Sci. Rev. 33, 233–275.

Emslie, A.G., Dennis, B.R., Holman, G.D., Hudson, H.S., 2005. Refinements to flare energy estimates: a followup to "Energy partition in two solar flare/CME events" by A. G. Emslie et al. J. Geophys. Res.(Space Phys.) 110, A11103.

Emslie, A.G., Kucharek, H., Dennis, B.R., Gopalswamy, N., Holman, G.D., Share, G.H., Vourlidas, A., Forbes, T.G., Gallagher, P.T., Mason, G.M., Metcalf, T.R., Mewaldt, R.A., Murphy, R.J., Schwartz, R.A., Zurbuchen, T.H., 2004. Energy partition in two solar flare/CME events. J. Geophys. Res. (Space Phys.) 109, A10104.

Eselevich, M.V., Eselevich, V.G., 2008. On formation of a shock wave in front of a coronal mass ejection with velocity exceeding the critical one. Geophys. Res. Lett. 35, L22105.

Eto, S., Isobe, H., Narukage, N., Asai, A., Morimoto, T., Thompson, B., Yashiro, S., Wang, T., Kitai, R., Kurokawa, H., Shibata, K., 2002. Relation between a Moreton wave and an EIT wave observed on 1997 November 4. Publ. Astron. Soc. Jpn. 54, 481–491.

Evans, R.M., Opher, M., Manchester IV, W.B., Gombosi, T.I., 2008. Alfvén profile in the lower corona: implications for shock formation. Astrophys. J. 687, 1355–1362.

Feldman, U., Widing, K.G., Warren, H.P., 1999. Morphology of the quiet solar upper atmosphere in the $4 \times 10^4 < T\_e < 1.4 \times 10^6$ K temperature regime. Astrophys. J. 522, 1133–1147.

Feng, L., Inhester, B., Solanki, S.K., Wiegelmann, T., Podlipnik, B., Howard, R.A., Wuelser, J., 2007. First stereoscopic coronal loop reconstructions from STEREO SECCHI images. Astrophys. J. 671, L205–L208.

Gallagher, P.T., Long, D.M., 2010. Large-scale bright fronts in the solar corona: a review of "EIT waves". ArXiv e-prints 1006.0140.

Gary, G.A., 2001. Plasma beta above a solar active region: rethinking the paradigm. Sol. Phys. 203, 71–86.

Gibson, S.E., Fan, Y., 2008. Partially ejected flux ropes: implications for interplanetary coronal mass ejections. J. Geophys. Res. (Space Phys.) 113, A09103.

Gilbert, H.R., Daou, A.G., Young, D., Tripathi, D., Alexander, D., 2008. The Filament-Moreton wave interaction of 2006 December 6. Astrophys. J. 685, 629–645.

Gilbert, H.R., Holzer, T.E., 2004. Chromospheric waves observed in the He I spectral line ($\lambda = 10830$ Å): a closer look. Astrophys. J. 610, 572–587.

Gilbert, H.R., Holzer, T.E., Thompson, B.J., Burkepile, J.T., 2004. A comparison of CME-associated atmospheric waves observed in coronal (Fe XII 195 Å) and chromospheric (He I 10830 Å) lines. Astrophys. J. 607, 540–553.

Gissot, S.F., Hochedez, J., Chainais, P., Antoine, J., 2008. 3D Reconstruction from SECCHI-EUVI images using an optical-flow algorithm: method description and observation of an erupting filament. Sol. Phys. 252, 397–408.

Golub, L., Deluca, E., Austin, G., Bookbinder, J., Caldwell, D., Cheimets, P., Cirtain, J., Cosmo, M., Reid, P., Sette, A., Weber, M., Sakao, T., Kano, R., Shibasaki, K., Hara, H., Tsuneta, S., Kumagai, K., Tamura, T., Shimojo, M., McCracken, J., Carpenter, J., Haight, H., Siler, R., Wright, E., Tucker, J., Rutledge, H., Barbera, M., Peres, G., Varisco, S., 2007. The X-ray telescope (XRT) for the Hinode mission. Sol. Phys. 243, 63–86.

Golub, L., Pasachoff, J.M., 2010. The Solar Corona. Cambridge University Press, Cambridge.

Gopalswamy, N., Yashiro, S., Temmer, M., Davila, J., Thompson, W.T., Jones, S., McAteer, R.T.J., Wuelser, J., Freeland, S., Howard, R.A., 2009. EUV wave reflection from a coronal hole. Astrophys. J. 691, L123–L127.

Gosling, J.T., 1993. The solar flare myth. J. Geophys. Res. 98, 18937–18950.

Grechnev, V.V., Uralov, A.M., Slemzin, V.A., Chertok, I.M., Kuzmenko, I.V., Shibasaki, K., 2008. Absorption Phenomena and a probable blast wave in the 13 July 2004 eruptive event. Sol. Phys. 253, 263–290.

Handy, B.N., Acton, L.W., Kankelborg, C.C., Wolfson, C.J., Akin, D.J., Bruner, M.E., Caravalho, R., Catura, R.C., Chevalier, R., Duncan, D.W., Edwards, C.G., Feinstein, C.N., Freeland, S.L., Friedlaender, F.M., Hoffmann, C.H., Hurlburt, N.E., Jurcevich, B.K., Katz, N.L., Kelly, G.A., Lemen, J.R., Levay, M., Lindgren, R.W., Mathur, D.P., Meyer, S.B., Morrison, S.J., Morrison, M.D., Nightingale, R.W., Pope, T.P., Rehse, R.A., Schrijver, C.J., Shine, R.A., Shing, L., Strong, K.T., Tarbell, T.D., Title, A.M., Torgerson, D.D., Golub, L., Bookbinder, J.A., Caldwell, D., Cheimets, P.N., Davis, W.N., Deluca, E.E., McMullen, R.A., Warren, H.P., Amato, D., Fisher, R., Maldonado, H., Parkinson, C., 1999. The transition region and coronal explorer. Sol. Phys. 187, 229–260.

Hansen, R.T., Garcia, C.J., Hansen, S.F., Yasukawa, E., 1974. Abrupt depletions of the inner corona. Publ. Astron. Soc. Pac. 86, 500–515.

Harra, L.K., Sterling, A.C., 2001. Material outflows from coronal intensity "dimming regions" during coronal mass ejection onset. Astrophys. J. 561, L215–L218.

Harra, L.K., Sterling, A.C., 2003. Imaging and spectroscopic investigations of a solar coronal wave: properties of the wave front and associated erupting material. Astrophys. J. 587, 429–438.

Harrison, R.A., 1995. The nature of solar flares associated with coronal mass ejection. Astron. Astrophys. 304, 585–594.

Harrison, R.A., 1996. Coronal magnetic storms: a new perspective on flares and the 'solar flare myth' debate. Sol. Phys. 166, 441–444.

Harrison, R.A., Bryans, P., Simnett, G.M., Lyons, M., 2003. Coronal dimming and the coronal mass ejection onset. Astron. Astrophys. 400, 1071–1083.

Harrison, R.A., Lyons, M., 2000. A spectroscopic study of coronal dimming associated with a coronal mass ejection. Astron. Astrophys. 358, 1097–1108.

Harrison, R.A., Sawyer, E.C., Carter, M.K., Cruise, A.M., Cutler, R.M., Fludra, A., Hayes, R.W., Kent, B.J., Lang, J., Parker, D.J., Payne, J., Pike, C.D., Peskett, S.C., Richards, A.G., Gulhane, J.L., Norman, K., Breeveld, A.A., Breeveld, E.R., AlJanabi, K.F., McCalden, A.J., Parkinson, J.H., Self, D.G., Thomas, P.D., Poland, A.I., Thomas, R.J., Thompson, W.T., Kjeldseth-Moe, O., Brekke, P., Karud, J., Maltby, P., Aschenbach, B., Bräuninger, H., Kühne, M., Hollandt, J., Siegmund, O.H.W., Huber, M.C.E.,

Gabriel, B.J.I., Mason, H.E., Bromage, B.J.I., 1995. The coronal diagnostic spectrometer for the solar and heliospheric observatory. Sol. Phys. 162, 233–290.

Harvey, K.L., Martin, S.F., Riddle, A.C., 1974. Correlation of a flare-wave and type II burst. Sol. Phys. 36, 151–155.

Hill, S.M., Pizzo, V.J., Balch, C.C., Biesecker, D.A., Bornmann, P., Hildner, E., Lewis, L.D., Grubb, R.N., Husler, M.P., Prendergast, K., Vickroy, J., Greer, S., Defoor, T., Wilkinson, D.C., Hooker, R., Mulligan, P., Chipman, E., Bysal, H., Douglas, J.P., Reynolds, R., Davis, J.M., Wallace, K.S., Russell, K., Freestone, K., Bagdigian, D., Page, T., Kerns, S., Hoffman, R., Cauffman, S.A., Davis, M.A., Studer, R., Berthiaume, F.E., Saha, T.T., Berthiume, G.D., Farthing, H., Zimmermann, F., 2005. The NOAA Goes-12 solar X-ray imager (SXI).1. Instrument, operations, and data. Sol. Phys. 226, 255–281.

Howard, R.A., Moses, J.D., Vourlidas, A., Newmark, J.S., Socker, D.G., Plunkett, S.P., Korendyke, C.M., Cook, J.W., Hurley, A., Davila, J.M., Thompson, W.T., St. Cyr, O.C., Mentzell, E., Mehalick, K., Lemen, J.R., Wuelser, J.P., Duncan, D.W., Tarbell, T.D., Wolfson, C.J., Moore, A., Harrison, R.A., Waltham, N.R., Lang, J., Davis, C.J., Eyles, C.J., Mapson-Menard, H., Simnett, G.M., Halain, J.P., Defise, J.M., Mazy, E., Rochus, P., Mercier, R., Ravet, M.F., Delmotte, F., Auchere, F., Delaboudiniere, J.P., Bothmer, V., Deutsch, W., Wang, D., Rich, N., Cooper, S., Stephens, V., Maahs, G., Baugh, R., McMullin, D., Carter, T., 2008. Sun earth connection coronal and heliospheric investigation (SECCHI). Space Sci. Rev. 136, 67–115.

Hudson, H.S., Acton, L.W., Freeland, S.L., 1996. A long-duration solar flare with mass ejection and global consequences. Astrophys. J. 470, 629–635.

Hudson, H.S., Cliver, E.W., 2001. Observing coronal mass ejections without coronagraphs. J. Geophys. Res. 106, 25199–25214.

Hudson, H.S., Khan, J.I., Lemen, J.R., Nitta, N.V., Uchida, Y., 2003. Soft X-ray observation of a large-scale coronal wave and its exciter. Sol. Phys. 212, 121–149.

Hudson, H.S., Warmuth, A., 2004. Coronal loop oscillations and flare shock waves. Astrophys. J. 614, L85–L88.

Hudson, H.S., Webb, D.F., 1997. Soft X-ray signatures of coronal ejections. In: Crooker, N., Joselyn, J., Feynman, J. (Eds.), Coronal Mass Ejections. AGU Geophysical Monograph Series, pp. 27–38.

Inhester, B., 2006. Stereoscopy basics for the STEREO mission. ArXiv Astrophysics e-prints arXiv:astro-ph/0612649.

Kahler, S.W., 1992. Solar flares and coronal mass ejections. Ann Rev. Astron. Astrophys. 30, 113–141.

Kai, K., McLean, D.J., 1968. Type II solar radio bursts observed with the Culgoora radioheliograph during a flare on 17 June 1968. Proc. Astron. Soc. Aust. 1, 141–142.

Kaiser, M.L., Kucera, T.A., Davila, J.M., St. Cyr, O.C., Guhathakurta, M., Christian, E., 2008. The STEREO mission: an introduction. Space Sci. Rev. 136, 5–16.

Khan, J.I., Aurass, H., 2002. X-ray observations of a large-scale solar coronal shock wave. Astron. Astrophys. 383, 1018–1031.

Kienreich, I.W., Temmer, M., Veronig, A.M., 2009. STEREO quadrature observations of the three-dimensional structure and driver of a global coronal wave. Astrophys. J. 703, L118–L122.

Klassen, A., Aurass, H., Mann, G., Thompson, B.J., 2000. Catalogue of the 1997 SOHO-EIT coronal transient waves and associated type II radio burst spectra. Astron. Astrophys. Suppl. 141, 357–369.

Klein, K., Khan, J.I., Vilmer, N., Delouis, J., Aurass, H., 1999. X-ray and radio evidence on the origin of a coronal shock wave. Astron. Astrophys. 346, L53–L56.

Kohl, J.L., Esser, R., Gardner, L.D., Habbal, S., Daigneau, P.S., Dennis, E.F., Nystrom, G.U., Panasyuk, A., Raymond, J.C., Smith, P.L., Strachan, L., van Ballegooijen, A.A., Noci, G., Fineschi, S., Romoli, M., Ciaravella, A., Modigliani, A., Huber, M.C.E., Antonucci, E., Benna, C., Giordano, S., Tondello, G., Nicolosi, P., Naletto, G., Pernechele, C., Spadaro, D., Poletto, G., Livi, S., vonderLühe, O., Geiss, J., Timothy, J.G., Gloeckler, G., Allegra, A., Basile, G., Brusa, R., Wood, B., Siegmund, O.H.W., Fowler, W., Fisher, R., Jhabvala, M., 1995. The ultraviolet coronagraph spectrometer for the solar and heliospheric observatory. Sol. Phys. 162, 313–356.

Krasnoselskikh, V., Podladchikova, O., 2007. Are EIT waves slow mode blast waves? AGU Fall Meeting Abstracts, A1047.

Landau, L.D., Lifshitz, E.M., 1987. Fluid Mechanics. Pergamon Press, Oxford.

Lin, R.P., Dennis, B.R., Hurford, G.J., Smith, D.M., Zehnder, A., Harvey, P.R., Curtis, D.W., Pankow, D., Turin, P., Bester, M., Csillaghy, A., Lewis, M., Madden, N., vanBeek, H.F., Appleby, M., Raudorf, T., McTiernan, J., Ramaty, R., Schmahl, E., Schwartz, R., Krucker, S., Abiad, R., Quinn, T., Berg, P., Hashii, M., Sterling, R., Jackson, R., Pratt, R., Campbell, R.D., Malone, D., Landis, D., Barrington-Leigh, C.P., Slassi-Sennou, S., Cork, C., Clark, D., Amato, D., Orwig, L., Boyle, R., Banks, I.S., Shirey, K., Tolbert, A.K., Zarro, D., Snow, F., Thomsen, K., Henneck, R., McHedlishvili, A., Ming, P., Fivian, M., Jordan, J., Wanner, R., Crubb, J., Preble, J., Matranga, M., Benz, A., Hudson, H., Canfield, R.C., Holman, G.D., Crannell, C., Kosugi, T., Emslie, A.G., Vilmer, N., Brown, J.C., Johns-Krull, C., Aschwanden, M., Metcalf, T., Conway, A., 2002. The Reuven Ramaty high-energy solar spectroscopic imager (RHESSI). Sol. Phys. 210, 3–32.

Linker, J., Mikic, Z., Riley, P., Lionello, R., Titov, V., 2008. Understanding eruptive phenomena with thermodynamic MHD simulations. In: Sa, S. (Ed.), 37th COSPAR Scientific Assembly, p. 1786.

Long, D.M., Gallagher, P.T., McAteer, R.T.J., Bloomfield, D.S., 2008. The kinematics of a globally propagating disturbance in the solar corona. Astrophys. J. 680, L81–L84.

Ma, S., Wills-Davey, M.J., Lin, J., Chen, P.F., Attrill, G.D.R., Chen, H., Zhao, S., Li, Q., Golub, L., 2009. A new view of coronal waves from STEREO. Astrophys. J. 707, 503–509.

Meyer, F., 1968. Flare-produced coronal waves. In: Kiepenheuer, K.O. (Ed.), Structure and Development of Solar Active Regions, pp. 485–489.

Moreton, G.E., 1960. Hα observations of flare-initiated disturbances with velocities 1000 km/sec. Astron. J. 65, 494–495.

Moreton, G.E., Ramsey, H.E., 1960. Recent observations of dynamical phenomena associated with solar flares. Publ. Astron. Soc. Pac. 72, 357–358.

Moreton, G.F., 1964. Hα Shock wave and winking filaments with the flare of 20 September 1963. Astron. J. 69, 145.

Moses, D., Clette, F., Delaboudinière, J., Artzner, G.E., Bougnet, M., Brunaud, J., Carabetian, C., Gabriel, A.H., Hochedez, J.F., Millier, F., Song, X.Y., Au, B., Dere, K.P., Howard, R.A., Kreplin, R., Michels, D.J., Defise, J.M., Jamar, C., Rochus, P., Chauvineau, J.P., Marioge, J.P., Catura, R.C., Lemen, J.R., Shing, L., Stern, R.A., Gurman, J.B., Neupert, W.M., Newmark, J., Thompson, B., Maucherat, A., Portier-Fozzani, F., Berghmans, D., Cugnon, P., vanDessel, E.L., Gabryl, J.R., 1997. EIT observations of the extreme ultraviolet Sun. Sol. Phys. 175, 571–599.

Muhr, N., Vršnak, B., Temmer, M., Veronig, A.M., Magdalenić, J., 2010. Analysis of a global moreton wave observed on 2003 October 28. Astrophys. J. 708, 1639–1649.

Murawski, K., Nakariakov, V.M., Pelinovsky, E.N., 2001. Fast magnetoacoustic waves in a randomly structured solar corona. Astron. Astrophys. 366, 306–310.

Narukage, N., Hudson, H.S., Morimoto, T., Akiyama, S., Kitai, R., Kurokawa, H., Shibata, K., 2002. Simultaneous observation of a moreton wave on 1997 November 3 in Hα and soft X-rays. Astrophys. J. 572, L109–L112.

Nelson, G.J., Melrose, D.B., 1985. Type II bursts. In: McLean, D.J., Labrum, N.R. (Eds.), Solar Radiophysics: Studies of Emission from the Sun at Metre Wavelengths, pp. 333–359.

Ofman, L., 2007. Three-dimensional MHD model of wave activity in a coronal active region. Astrophys. J. 655, 1134–1141.

Ofman, L., Thompson, B.J., 2002. Interaction of EIT waves with coronal active regions. Astrophys. J. 574, 440–452.

Ontiveros, V., Vourlidas, A., 2009. Quantitative measurements of coronal mass ejection-driven shocks from LASCO Observations. Astrophys. J. 693, 267–275.

Parker, E.N., 1961. Sudden expansion of the corona following a large solar flare and the attendant magnetic field and cosmic-ray effects. Astrophys. J. 133, 1014–1033.

Patsourakos, S., Vourlidas, A., 2009. "Extreme ultraviolet waves" are waves: first quadrature observations of an extreme ultraviolet wave from STEREO. Astrophys. J. 700, L182–L186.

Patsourakos, S., Vourlidas, A., Wang, Y.M., Stenborg, G., Thernisien, A., 2009. What is the nature of EUV waves? First STEREO 3D observations and comparison with theoretical models. Sol. Phys. 259, 49–71.

Pettit, E., 1919. The great eruptive prominences of May 29 and July 15. Astrophys. J. 50, 206–219.

Phillips, K.J.H., Feldman, U., Landi, E., 2008. Ultraviolet and X-ray Spectroscopy of the Solar Atmosphere. Cambridge University Press.

Pick, M., Malherbe, J., Kerdraon, A., Maia, D.J.F., 2005. On the disk H α and radio observations of the 2003 October 28 flare and coronal mass ejection event. Astrophys. J. 631, L97–L100.

Podladchikova, O., Berghmans, D., 2005. Automated detection of EIT waves and dimmings. Sol. Phys. 228, 265–284.

Podladchikova, O., Vourlidas, A., Van der Linden, R.A.M., Wülser, J., Patsourakos, S., 2010. Extreme ultraviolet observations and analysis of micro-eruptions and their associated coronal waves. Astrophys. J. 709, 369–376.

Pohjolainen, S., Maia, D., Pick, M., Vilmer, N., Khan, J.I., Otruba, W., Warmuth, A., Benz, A., Alissandrakis, C., Thompson, B.J., 2001. On-the-disk development of the halo coronal mass ejection on 1998 May 2. Astrophys. J. 556, 421–431.

Polovin, R.V., 1961. Reviews of topical problems: shock waves in magnetohydrodynamics. Sov. Phys. Usp. 3, 677–688.

Pomoell, J., Vainio, R., Kissmann, R., 2008. MHD modeling of coronal large-amplitude waves related to CME lift-off. Sol. Phys. 253, 249–261.

Priest, E.R., Forbes, T.G., 2002. The magnetic nature of solar flares. Astron. Astrophys. Rev. 10, 313–377.

Robbrecht, E., Verwichte, E., Berghmans, D., Hochedez, J.F., Poedts, S., Nakariakov, V.M., 2001. Slow magnetoacoustic waves in coronal loops: EIT and TRACE. Astron. Astrophys. 370, 591–601.

Rodriguez, L., Zhukov, A.N., Gissot, S., Mierla, M., 2009. Three-dimensional reconstruction of active regions. Sol. Phys. 256, 41–55.

Roussev, I.I., Lugaz, N., Sokolov, I.V., 2007. New physical insight on the changes in magnetic topology during coronal mass ejections: case studies for the 2002 April 21 and August 24 events. Astrophys. J. 668, L87–L90.

Rust, D.M., Hildner, E., 1976. Expansion of an X-ray coronal arch into the outer corona. Sol. Phys. 48, 381–387.

Rust, D.M., Svestka, Z., 1979. Slowly moving disturbances in the X-ray corona. Sol. Phys. 63, 279–295.

Sakao, T., Kano, R., Narukage, N., Kotoku, J., Bando, T., DeLuca, E.E., Lundquist, L.L., Tsuneta, S., Harra, L.K., Katsukawa, Y., Kubo, M., Hara, H., Matsuzaki, K., Shimojo, M., Bookbinder, J.A., Golub, L., Korreck, K.E., Su, Y., Shibasaki, K., Shimizu, T., Nakatani, I., 2007. Continuous plasma outflows from the edge of a solar active region as a possible source of solar wind. Science 318, 1585–1588.

Schmidt, J.M., Ofman, L., 2010. Global simulation of an extreme ultraviolet imaging telescope wave. Astrophys. J. 713, 1008–1015.

Schwenn, R., dal Lago, A., Huttunen, E., Gonzalez, W.D., 2005. The association of coronal mass ejections with their effects near the earth. Ann. Geophys. 23, 1033–1059.

Sedov, L.I., 1959. Similarity and Dimensional Methods in Mechanics. Academic Press, New York.

Sheeley, N.R., Hakala, W.N., Wang, Y., 2000. Detection of coronal mass ejection associated shock waves in the outer corona. J. Geophys. Res. 105, 5081–5092.

Smith, S.F., Harvey, K.L., 1971. Observational effects of flare-associated waves. In: Macris, C.J. (Ed.), Physics of the Solar Corona. p. 156.

Steinolfson, R.S., Wu, S.T., Dryer, M., Tandberg-Hanssen, E., 1978. Magnetohydrodynamic models of coronal transients in the meridional plane. I—the effect of the magnetic field. Astrophys. J. 225, 259–274.

Sterling, A.C., Hudson, H.S., 1997. YOHKOH SXT observations of X-ray "dimming" associated with a halo coronal mass ejection. Astrophys. J. 491, L55–L58.

Thernisien, A.F.R., Howard, R.A., Vourlidas, A., 2006. Modeling of flux rope coronal mass ejections. Astrophys. J. 652, 763–773.

Thompson, B.J., Cliver, E.W., Nitta, N., Delannée, C., Delaboudinière, J.P., 2000a. Coronal dimmings and energetic CMEs in April–May 1998. Geophys. Res. Lett. 27, 1431–1434.

Thompson, B.J., Gurman, J.B., Neupert, W.M., Newmark, J.S., Delaboudinière, J.P., St. Cyr, O.C., Stezelberger, S., Dere, K.P., Howard, R.A., Michels, D.J., 1999. SOHO/EIT observations of the 1997 April 7 coronal transient: possible evidence of coronal Moreton waves. Astrophys. J. 517, L151–L154.

Thompson, B.J., Myers, D.C., 2009. A catalog of coronal "EIT wave" transients. Astrophys. J. Suppl. Ser. 183, 225–243.

Thompson, B.J., Plunkett, S.P., Gurman, J.B., Newmark, J.S., St. Cyr, O.C., Michels, D.J., Delaboudinière, J.P., 1998. SOHO/EIT observations of an earth-directed coronal mass ejection 12, 2461–2464.

Thompson, B.J., Reynolds, B., Aurass, H., Gopalswamy, N., Gurman, J.B., Hudson, H.S., Martin, S.F., St. Cyr, O.C., 2000b. Observations of the 24 September 1997 coronal flare waves. Sol. Phys. 193, 161–180.

Title, A.M., AIA team, 2006. The atmospheric imaging assembly on the solar dynamics observatory. In: Bulletin of the American Astronomical Society. p. 261.

Tripathi, D., Raouafi, N., 2007. On the relationship between coronal waves associated with a CME on 5 March 2000. Astron. Astrophys. 473, 951–957.

Tsuneta, S., Acton, L., Bruner, M., Lemen, J., Brown, W., Caravalho, R., Catura, R., Freeland, S., Jurcevich, B., Owens, J., 1991. The soft X-ray telescope for the SOLAR-A mission. Sol. Phys. 136, 37–67.

Uchida, Y., 1968. Propagation of hydromagnetic disturbances in the solar corona and Moreton's wave phenomenon. Sol. Phys. 4, 30–44.

Uchida, Y., 1970. Diagnosis of coronal magnetic structure by flare-associated hydromagnetic disturbances. Publ. Astron. Soc. Jpn. 22, 341–364.

Uchida, Y., 1974. Behavior of the flare produced coronal MHD wavefront and the occurrence of type II radio bursts. Sol. Phys. 39, 431–449.

Uchida, Y., Altschuler, M.D., Newkirk, G.J., 1973. Flare-produced coronal MHD-fast-mode wavefronts and Moreton's wave phenomenon. Sol. Phys. 28, 495–516.

Veronig, A.M., Muhr, N., Kienreich, I.W., Temmer, M., Vršnak, B., 2010. First observations of a dome-shaped large-scale coronal extreme-ultraviolet wave. Astrophys. J. 716, L57–L62.

Veronig, A.M., Temmer, M., Vršnak, B., 2008. High-cadence observations of a global coronal wave by STEREO EUVI. Astrophys. J. 681, L113–L116.

Veronig, A.M., Temmer, M., Vršnak, B., Thalmann, J.K., 2006. Interaction of a Moreton/EIT wave and a coronal hole. Astrophys. J. 647, 1466–1471.

Vourlidas, A., Wu, S.T., Wang, A.H., Subramanian, P., Howard, R.A., 2003. Direct detection of a coronal mass ejection-associated shock in large angle and spectrometric coronagraph experiment white-light images. Astrophys. J. 598, 1392–1402.

Vršnak, B., Cliver, E.W., 2008. Origin of coronal shock waves. Invited Review. Sol. Phys. 253, 215–235.

Vršnak, B., Lulić, S., 2000a. Formation of coronal MHD shock waves—I. The basic mechanism. Solar Phys. 196, 157–180.

Vršnak, B., Lulić, S., 2000b. Formation of coronal MHD shock waves—II. The pressure pulse mechanism. Sol. Phys. 196, 181–197.

Vršnak, B., Magdalenić, J., Temmer, M., Veronig, A., Warmuth, A., Mann, G., Aurass, H., Otruba, W., 2005. Broadband metric-range radio emission associated with a Moreton/EIT wave. Astrophys. J. 625, L67–L70.

Vršnak, B., Warmuth, A., Brajša, R., Hanslmeier, A., 2002. Flare waves observed in helium i 10 830 Å. A link between Hα Moreton and EIT waves. Astron. Astrophys. 394, 299–310.

Vršnak, B., Warmuth, A., Temmer, M., Veronig, A., Magdalenić, J., Hillaris, A., Karlický, M., 2006. Multi-wavelength study of coronal waves associated with the CME-flare event of 3 November 2003. Astron. Astrophys. 448, 739–752.

Wang, H., Shen, C., Lin, J., 2009. Numerical experiments of wave-like phenomena caused by the disruption of an unstable magnetic configuration. Astrophys. J. 700, 1716–1731.

Wang, Y., Sheeley, N.R., Socker, D.G., Howard, R.A., Rich, N.B., 2000. The dynamical nature of coronal streamers. J. Geophys. Res. 105, 25133–25142.

Wang, Y.M., 2000. EIT waves and fast-mode propagation in the solar corona. Astrophys. J. 543, L89–L93.

Warmuth, A., 2007. Large-scale waves and shocks in the solar corona. In: Klein, K.-L., MacKinnon A.L. (Eds.), Lecture Notes in Physics. Springer Verlag, Berlin, pp. 107-138.

Warmuth, A., 2010. Large-scale waves in the solar corona: the continuing debate. Adv. Space Res. 45, 527–536.

Warmuth, A., Mann, G., Aurass, H., 2005. First soft X-ray observations of global coronal waves with the goes solar X-ray imager. Astrophys. J. 626, L121–L124.

Warmuth, A., Vršnak, B., Aurass, H., Hanslmeier, A., 2001. Evolution of two EIT/Hα Moreton waves. Astrophys. J. 560, L105–L109.

Warmuth, A., Vršnak, B., Magdalenić, J., Hanslmeier, A., Otruba, W., 2004a. A multiwavelength study of solar flare waves. I. Observations and basic properties. Astron. Astrophys. 418, 1101–1115.

Warmuth, A., Vršnak, B., Magdalenić, J., Hanslmeier, A., Otruba, W., 2004b. A multiwavelength study of solar flare waves. II. Perturbation characteristics and physical interpretation. Astron. Astrophys. 418, 1117–1129.

Weiss, A.A., 1963. The positions and movements of the sources of solar radio bursts of spectral type II. Aust. J. Phys. 16, 240–271.

Weiss, A.A., Sheridan, K.V., 1962. The sizes of the sources of solar radio bursts at 40 and 60 mc/s. J. Phys. Soc. Jpn. 17, 223–227.

White, S.M., Thompson, B.J., 2005. High-cadence radio observations of an EIT wave. Astrophys. J. 620, L63–L66.

Wild, J.P., McCready, L.L., 1950. Observations of the spectrum of high-intensity solar radiation at metre wavelengths. I. The apparatus and spectral types of solar burst observed. Aust. J. Sci. Res. A Phys. Sci. 3, 387–398.

Wild, J.P., Sheridan, K.V., Kai, K., 1968. 80 Mhz photography of the eruption of a solar prominence. Nature 218, 536–539.

Wills-Davey, M.J., 2003. Propagating disturbances in the lower solar corona. Ph.D. Thesis. Montana State University.

Wills-Davey, M.J., 2006. Tracking large-scale propagating coronal wave fronts (EIT waves) using automated methods. Astrophys. J. 645, 757–765.

Wills-Davey, M.J., Attrill, G.D.R., 2009. EIT waves: a changing understanding over a solar cycle. Space Sci. Rev. 149, 325–353.

Wills-Davey, M.J., DeForest, C.E., Stenflo, J.O., 2007. Are EIT waves fast-mode MHD waves? Astrophys. J. 664, 556–562.

Wills-Davey, M.J., Thompson, B.J., 1999. Observations of a propagating disturbance in trace. Sol. Phys. 190, 467–483.

Wu, S.T., Li, B., Wang, S., Zheng, H., 2005. A three-dimensional analysis of global propagation of magnetohydrodynamic (MHD) waves in a structured solar atmosphere. J. Geophys. Res. (Space Phys.) 110, A11102.

Wu, S.T., Zheng, H., Wang, S., Thompson, B.J., Plunkett, S.P., Zhao, X.P., Dryer, M., 2001. Three-dimensional numerical simulation of MHD waves observed by the extreme ultraviolet imaging telescope. J. Geophys. Res. 106, 25089–25102.

Yang, H.Q., Chen, P.F., 2010. The dependence of the EIT wave velocity on the magnetic field strength. Sol. Phys. 266, 59–69.

Zarro, D.M., Sterling, A.C., Thompson, B.J., Hudson, H.S., Nitta, N., 1999. SOHO EIT observations of extreme-ultraviolet "dimming" associated with a halo coronal mass ejection. Astrophys. J. 520, L139–L142.

Zel'dovich, Y.B., Raizer, Y.P., 1967. Physics of Shock Waves and High-Temperature Hydrodynamic Phenomena. Academic Press, New York.

Zhang, J., Dere, K.P., 2006. A statistical study of main and residual accelerations of coronal mass ejections. Astrophys. J. 649, 1100–1109.

Zhang, J., Dere, K.P., Howard, R.A., Kundu, M.R., White, S.M., 2001. On the temporal relationship between coronal mass ejections and flares. Astrophys. J. 559, 452–462.

Zhukov, A.N., 2004. Initiation of CMEs: EIT waves and EUV dimmings. In: T. Sakurai, T. Sekii (Eds.), The Solar-B Mission and the Forefront of Solar Physics. pp. 381–388.

Zhukov, A.N., Auchère, F., 2004. On the nature of EIT waves, EUV dimmings and their link to CMEs. Astron. Astrophys. 427, 705–716.

Zhukov, A.N., Rodriguez, L., de Patoul, J., 2009. STEREO/SECCHI observations on 8 December 2007: evidence against the wave hypothesis of the EIT wave origin. Sol. Phys. 259, 73–85.

Zhukov, A.N., Veselovsky, I.S., 2007. Global coronal mass ejections. Astrophys. J. 664, L131–L134.

Žic, T., Vršnak, B., Temmer, M., Jacobs, C., 2008. Cylindrical and spherical pistons as drivers of MHD shocks. Sol. Phys. 253, 237–247.